Surface drift in the South Pacific Gyre: Observations and simulations of drifters and plastic

Master Thesis

Astrid Bergland

Geophysical Institute
Faculty of Mathematics and Natural Sciences
University of Bergen

August 2022

Acknowledgements

I want to thank my supervisors, Øyvind Breivik and Cecilie Mauritzen, for guiding me through this project. A special thank you to Graig Sutherland for helping me with the leeway coefficients and the discussions around the method.

I would also like to express my deepest gratitude to my dad for being a good discussion partner when I felt stuck. A big thank you to Astrid and Carina for giving me a place to stay during the last week of writing this thesis and to my friends who have read enough of it to be sick of it. I would also like to thank my family and friends for providing me with unfailing support and encouragement throughout my years of study and through the process of writing this thesis. This could not have been possible without them. Finally, I would like to thank Kristian for all the late-night pep talks and all the reminders of the importance of using pprint when coding. Thank you.

Abstract

The objective of this thesis is to investigate the residence times and behavior of microplastics and macroplastics in the southern Pacific Ocean. I use the open-source Lagrangian particle tracking framework OpenDrift to reproduce drifter trajectories and simulate the large-scale drift of marine plastic in the south pacific subtropical gyre. I conducted three different simulations. First, I conducted simulations to assess of how well the ORAS5, ERA5, and OpenDrift reproduced the observed drifter trajectories from the Kon-Tiki 2 expedition before and after they lost their drogue and until they stopped transmitting. The results showed that ORAS5 did a varying job in reproducing the undrogued drifters but a better job reproducing the drogued. This result was as expected because no wind effects were included in those simulations as the leeway coefficient was estimated to be less than 1%. From the simulation of the drift of micro- and macroplastics using Lagrangian particle tracking with ocean and atmospheric forcing from reanalysis products, I find that microplastic and macroplastic accumulate in the eastern part of the South Pacific and forms a well-defined plastic gyre within 12 years. After the plastic reaches the accumulation zone, the zone and borders are not stationary in time but vary in shape and location. However, the minimal number of plastic particles within the zones are relatively steady, indicating that there is no, or only minimal, leakage of plastic over the final 12 years of simulation. The seasonal variation of the particles crossing the 30°S line is more prominent in the micro than in the macro simulation. On top of the seasonal variability, there seems to be a signal on a longer time scale, which might be an ENSO signal, but this would need further investigation.

Contents

1 Introduction

Marine plastic debris is a growing global threat to the marine environment. The first reports on marine plastic contamination came in the 1970s, less than two decades after the rise of commercial plastic production (Law, 2017). Plastic pollution is found widespread throughout the world's oceans, but the magnitude of marine plastic is not easily quantified. It is estimated that around 5-12 tonnes of plastic enter the ocean from land-based sources each year (Jambeck et al., 2015). However, estimates of the total amount of plastic floating in the ocean are close to 0.3 million tonnes (Cózar et al. (2014), Eriksen et al. (2014), Van Sebille et al. (2015)). Thus there is a huge discrepancy in how much plastic enters the ocean compared to the observations, therefore more studies are needed to find out where it goes.

Plastic is not biodegradable, but can break into smaller pieces by currents and waves. As a result, marine plastic debris comes in many sizes, ranging from macro to nanoscales (Zaki and Aris, 2022). This resistance to degradation results in long residence times when plastic is introduced into the marine environment (Andrady, 2011). These long residence times and the relatively high buoyancy are generally assumed to be reasons why we find plastic so far away from its sources (Andrady, 2005). Observations have shown that plastic has a tendency to accumulate on the eastern side of subtropical gyres (Cózar et al. (2014), Eriksen et al. (2013), Law et al. (2014)). The tendency for accumulation has been found to be caused by surface Ekman currents pushing the plastic towards the middle of the wind-driven gyre in the Pacific (Martinez et al. (2009), Onink et al. (2019)). In order to get a better understanding of how the plastic enters such a closed system as the South Pacific garbage patch, I will use the trajectory model framework OpenDrift (Dagestad et al., 2018), together with the reanalyses ORAS5 and ERA5. Martinez et al. (2009) used satellite-derived SSH and wind stress fields from the period 1993 to 2001 to determine the surface circulation of the South Pacific and then computed the Lagrangian trajectories of floating debris. Starting with debris particles placed in a uniform grid their model simulation resulted in accumulation in the eastern center of the South Pacific gyre. In the first two years, mostly forced by Ekman drift, the debris drifted towards the tropical convergence zone, then advected eastward mostly by geostrophic currents. They finally reach the eastern central region of the South Pacific gyre, where Martinez et al. (2009) concludes that the particles could not escape.

I use a similar framework based on an initial uniform distribution of plastic particles in the Pacific and a long term simulation using reanalysis data for the period 1993 through 2019. My study differs from Martinez et al. (2009), as I look at the drift of both microplastics and macroplastic over a 20 year period. The results of my research collaborate the previous work by Martinez that there is an accumulation zone in the South Pacific gyre from which very little debris escapes once trapped.

As I use two reanalysis products to study the drift of marine debris, it is essential to check if they reproduce the trajectory of objects satisfactorily. Surface drifting buoys or drifters have a long history in oceanography to map currents and following particles and objects moving in the ocean (Lumpkin et al., 2017). Therefore I will use drifters deployed during the Kon-Tiki 2 expedition in 2015 to evaluate how adequately the reanalyses perform. In several recent studies, drifters from the Global Drifter Program (Niiler (2001),Lumpkin et al. (2017)) have been used to study the pathways of ma-

rine plastic debris (Maximenko et al. (2012), Lumpkin et al. (2012), Van Sebille et al. (2015)). Therefore, if the reanalysis and OpenDrift sufficiently reproduce the drifter pathways, it would most likely be accurate enough for large-scale simulations of plastic drift.

The drifters that the Kon-Tiki 2 expedition released had a drogue centered at 15-meters depth attached to the surface buoy, which makes the drifter follow the current at 15 meters. The drogues tend to fall off; consequently, the drifter velocity is tainted with wind drift (Menna et al., 2018). In order to estimate the wind drift on the drogueless drifters, I utilize the method proposed by Sutherland et al. (2020). This method predicts the wind drift by interpolating the flow fields to the drifter positions, giving leeway coefficients that vary in both time and direction. Thus, the time series of these coefficients reproduce the drifter trajectories perfectly. The mean of this time series will be taken as the leeway coefficient.

In this thesis, I aim to answer the following key questions: how does the ocean circulation, combined with the prevailing winds, distribute plastic? Which part of the southern pacific retains the highest amount of plastic? I use drifters to assess the performance of the ocean reanalysis. I also estimate the wind drift of the undrogued drifters using a novel method involving the reanalysis products. The thesis is structured as follows. Section 2 presents a short introduction to the current systems and variability in the South Pacific. Details of the drifters and reanalyses are found in section 3.1, and the experiments in section 3.2. Results are presented in section 4. The results are discussed in section 5 followed by a short conclusion in section 6.

2 Study Area

The wind stress mainly drives the upper ocean circulation in the South Pacific (Talley et al., 2011). The prevailing winds form a large anticyclonic subtropical gyre bounded by currents (Figure 1). In the west, the western boundary current, the East Australian Current, flows southwards along the coast of Australia until it reaches the northern-most point of New Zealand. Here the East Australian Current separates, and one part continues southwards to Tasmania, and the other continues around the coastline around New Zealand, forming the East Auckland Current (Roemmich and Sutton, 1998). The East Auckland Current joins the South Pacific Current, the large eastern flowing part of the subtropical gyre (Stramma et al., 1995) The Antarctic Circumpolar Current bounds the southern part of the gyre, with the Subantarctic front.

On the eastern side of the basin, the Peru-Chile Current flows along the coast of South America. In the north, the strong westward South Equatorial Current closes the gyre. The wind-driven circulation is primarily driven by the easterly Trade Winds north of 30°S and by the Westerlies south of this. This sets up a southwards Ekman transport by the Trade Winds and a northwards Ekman transport by the Westerlies, thus there is Ekman convergence throughout the subtropical South Pacific.

The South Pacific is home to The El Niño-Southern Oscillation (ENSO), one of the most studied phenomena in climate and it contributes greatly to the inter-annual climate variability. The phenomenon is characterized by two phases, anomalous warming (El Niño) and anomalous cooling (La Niña) of the surface water around the equator. These occur every 2 to 7 years and vary in strength. During an El Niño year, the Trade Winds are weakened and may even be reversed, thus ENSO is an important part of the variability in the South Pacific Gyre as it is driven by the Trade winds. Figure 2 shows the National Oceanic and Atmospheric Administration (NOAA) Niño 3.4 index (Rayner et al., 2003) as well as the calculated index for ORAS5 over the period from 1993 to 2019 Figure 2. The Niño 3.4 index is the sea surface temperature anomalies averaged over a region in the equatorial Pacific. If the anomalies exceed $\pm$ 0.4°C over a period of 6 months.

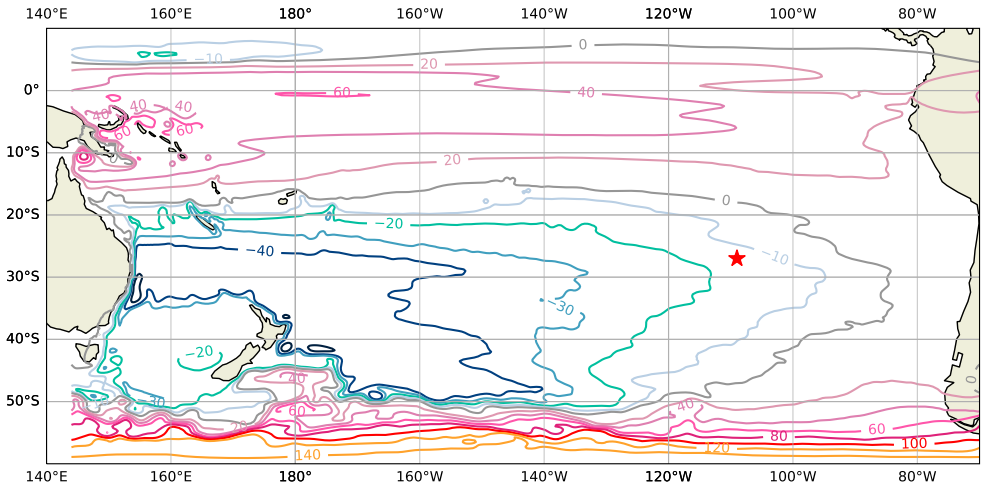

Figure 1: Temporal mean barotropic stream function for the upper 1000 meters in ORAS5, calculated using the python package *windspharm* (Dawson, 2016). Since this package is meant for computing stream functions for the atmosphere, there is nonphysical flow going through the boundaries.

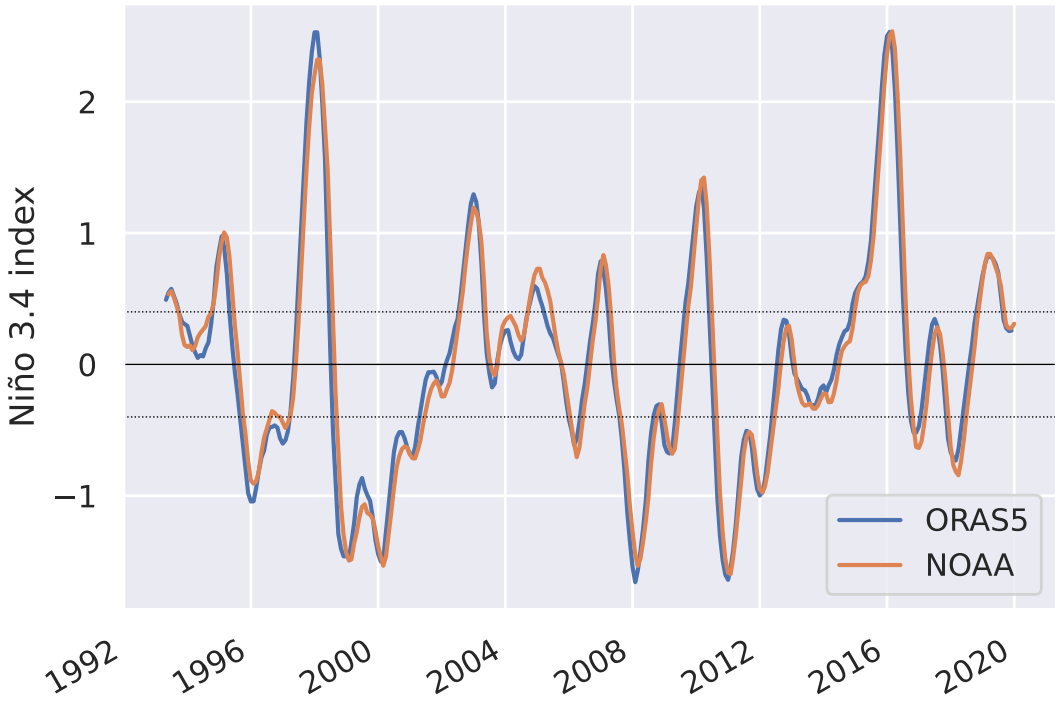

Figure 2: Calculated Nino 3.4 index for ORAS5 (blue line) and the NOAA index (Rayner et al., 2003) in orange.

3 Data and Method

3.1 Data

3.1.1 Drifters

As a part of the scientific program aboard the Kon-Tiki 2 expedition, 16 drifters from the Global Drifter Program were deployed in pairs on the voyage from Lima to Rapa Nui. From late November to mid-December 2015. The drifter data is available as hourly interpolated data (Elipot et al., 2016). An overview of the drifters is presented in Table 1 and the drifter trajectories in Figure 3. The drifters deployed were standardized Surface Velocity Program (SVP) drifters (Niiler et al., 1995). The drifter design consists of a spherical surface float and a "holey sock" drogue. The purpose of the drogue is to minimize the motion caused by the surface-wave-driven Stokes layer and remain unaffected by direct wind forcing. It is centered at 15 meters depth. The drogue frequently pulls the surface float beneath the surface, whereas a drogueless float remains at the surface. Therefore the drifters are equipped with a tether strain sensor for drogue detection. I filtered out the drifters that stopped transmitting within a year. From the 16 drifters deployed one never started transmitting.

Table 1: Drifter metadata with date and location of deployment and date and location of transmission. Type of death describes the fate of the drifter. (1 = buoy ran aground, 2 = buoy picked up, 3 = stopped transmitting)

	Deploy			End			Type	Drogue
ID	Date	Longitude	Latitude	Date	Longitude	Latitude	Death	Lost Date
139566	2015-11-12	-80.638	-11.480	2016-03-10	-82.070	-17.800	1	-
139799	2015-11-16	-84.005	-11.870	2015-12-18	-87.000	-12.570	2	-
139563	2015-11-16	-84.005	-11.870	2017-04-01	-137.000	-18.280	1	2015-11-29
139617	2015-11-17	-85.090	-11.967	2017-04-16	-141.680	-22.630	3	2016-06-09
139895	2015-11-20	-87.492	-12.695	2017-03-11	-141.190	-19.210	1	2016-02-28
139619	2015-11-20	-87.475	-12.695	2019-01-31	146.350	-17.840	2	2016-08-06
139562	2015-11-24	-91.750	-14.123	2019-10-07	-106.800	-26.120	3	2017-03-05
139564	2015-11-28	-95.067	-16.183	2018-03-29	-120.780	-29.010	3	2016-12-29
139565	2015-11-28	-95.067	-16.183	2019-08-16	-109.350	-28.970	3	-
139794	2015-12-02	-98.892	-18.793	2018-06-28	-128.560	-24.200	3	2016-06-07
139800	2015-12-02	-98.892	-18.793	2019-10-13	-87.640	-29.070	3	2016-10-03
139908	2015-12-08	-101.870	-22.085	2018-08-02	-120.820	-30.420	3	2016-08-10
139793	2015-12-08	-101.870	-22.085	2019-11-15	-107.760	-27.310	3	2016-07-31
139909	2015-12-14	-105.665	-25.312	2018-10-20	-104.370	-30.370	3	2017-05-21
139798	2015-12-14	-105.665	-25.312	2019-10-03	-100.630	-25.040	3	2016-06-06

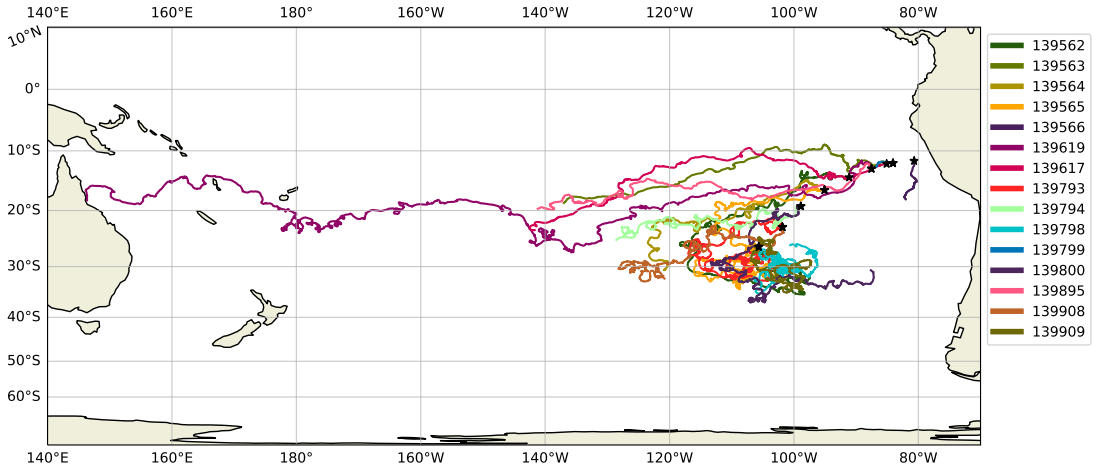

Figure 3: An overview of the trajectories for the drifters released during the first leg of the Kon-Tiki 2 expedition. The drifters are differentiated with various colors. The black star indicates the deployment positions.

3.1.2 ORAS5

The ORAS5 (Zuo et al., 2019) reanalysis is a historical reconstruction of the ocean and sea ice state from 1979 to the present by the European Center for Medium-Range Weather Forecasts (ECMWF). It is an ensemble consisting of 5 members. The reanalysis is produced by a coupled ocean-ice model driven by atmospheric forcing and constrained via a data assimilation method of ocean observations. The atmospheric forcing fields are from the atmospheric reanalysis ERA-Interim (Berrisford et al., 2009) until 2015 and from the EMCWF operational numerical weather prediction afterward (Zuo et al., 2019). The ORAS5 is then reprocessed with ERA-Interim forcing before making it available as a part of the ensemble of global reanalyses distributed by Copernicus Marine Service, with a time resolution of daily means (`https://doi.org/10.48670/moi-00024`). The horizontal resolution of ORAS5 is approximately 0.25°on a stretched grid, here interpolated to a regular grid of 0.25°. There are 75 unevenly spaced vertical levels from -5500 to 0 meters, with a higher density of layers close to the surface. In this thesis, the current fields and the sea surface temperature is used with a temporal subset from 1993 to 2019. The averaged surface currents over the time period are shown in Figure 4.

3.1.3 ERA5

For the atmospheric forcing and the Stokes drift, fields from the atmospheric reanalysis ERA5 (Hersbach et al., 2020) produced by the ECMWF were used. ERA5 replaced ERA-Interim, with an increased vertical and horizontal resolution, as well as having consistent sea surface temperature records with ORAS5. The ERA5 is a coupled atmosphere-wave model. The atmospheric horizontal resolution is 31 km, while the wave fields have a resolution of 50 km. The reanalysis has an hourly temporal resolution. The data is available from 1959 to the present day, but in this thesis, I will use a

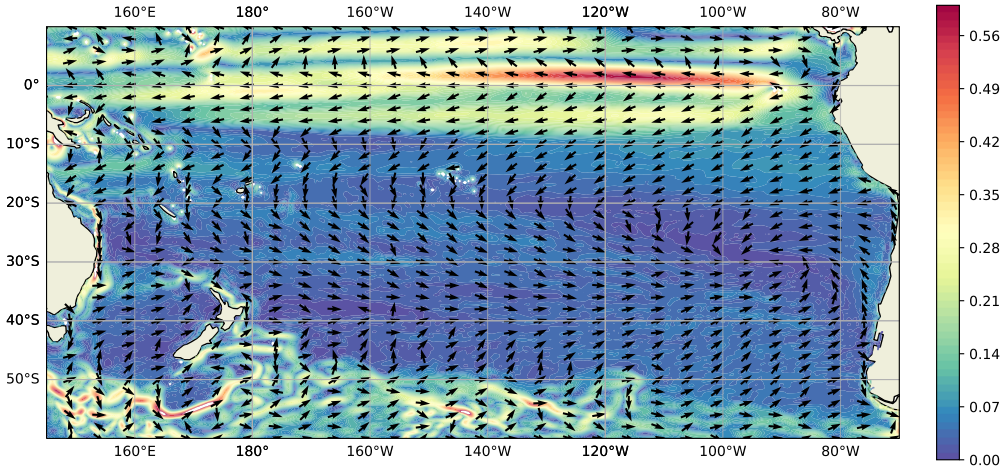

Figure 4: Temporal mean of the surface currents in ORAS5. The average is taken for the period from 1993 to 2019, with normalized vectors to indicate the mean direction and a color map to indicate the magnitude.

subset from 1993 to 2019. The subset has a temporal resolution of 3 hours to solve for the synoptic scale. The horizontal scale is interpolated to a 0.25°grid in order to match the resolution of ORAS5.

3.2 Method

3.2.1 Lagrangian Particle Tracking: OpenDrift

In this thesis, I use the open-source Lagrangian particle tracking framework OpenDrift (Dagestad et al., 2018) to reproduce drifter trajectories and simulate the large-scale drift of marine plastic. This section gives a short introduction to the Lagrangian description and OpenDrift.

In fluid dynamics, the fluid motion can be described in two different ways, either by looking at the properties of the fluid at fixed points, the Eulerian view or by looking at the motion in terms of the properties of different fluid parcels each identified by some label, the Lagrangian view (Vallis, 2017). Both approaches provide a complete description of the fluid dynamical system. Nevertheless, the Eulerian approach is more widely used as we are typically more interested in the weather where we live than where it comes from and where it goes. Most numerical models are based on this formulation. However, when studying the pathways of objects in the ocean, the Lagrangian approach is more practical as it allows us to follow the object through time and space. A common analogy to visualize the Lagrangian formulation is to imagine being in a hot-air balloon, following the winds, and noting your position. The movement of the balloon can then be described by its position vector, $\boldsymbol{x} = \boldsymbol{x}(\boldsymbol{x}(t = t_0), t)$ or $\boldsymbol{x} = \boldsymbol{x}(\boldsymbol{a}, t)$ where $\boldsymbol{a} = \boldsymbol{x}(t = t_0)$ is the initial position. This curve in space is called a trajectory (van Sebille et al., 2018). In the Lagrangian description, time and initial position $\boldsymbol{a}$ are the independent variables and the position vector $\boldsymbol{x}$ is the dependent variable (Bennett, 2006). Thus the Lagrangian velocity is:

$$\mathbf{v}_l = \left. \frac{d\mathbf{x}(\mathbf{a}, t)}{dt} \right|_{\mathbf{a}} \tag{1}$$

The object's position is updated by

$$\mathbf{x}(t + \Delta t) = \mathbf{x}(t) + \int_t^{t+\Delta t} \mathbf{v}_e(\mathbf{x}(\tau), \tau) d\tau. \tag{2}$$

where τ is the time interval in the Eulerian domain (van Sebille et al., 2018).

There are two commonly used ways to compute the Lagrangian integration: the online and the offline approach. In the online approach, trajectories are computed along with the velocity fields each time the Eulerian model updates. For the offline approach, the trajectories are computed by velocity outputs from Eulerian models or observation-based surface velocities. Some advantages of an offline computation is that the particles can be forced with velocity fields from multiple models, meaning that ocean forcings can be induced by one model and atmospheric forcing from another. Other notable advantages are that modifications can be done quickly and that computations can be run backwards in time (van Sebille et al., 2018).

OpenDrift is an open-sourced offline Lagrangian particle tracking framework developed at the Norwegian Meteorological Institute (Dagestad et al., 2018). The framework is python based and readily available at `https://opendrift.github.io`. The framework is designed to be generic and modular to accommodate a wide range of drift calculations in the ocean or atmosphere. Some of these modules include *OpenOil*

for oil drift, *Leeway* for search and rescue, and *OceanDrift* being the most basic of the modules used for tracking water masses or passive tracers. I will use the latter for all the simulations and experiments in this thesis. *OceanDrift* allows for the inclusion of both Stokes drift and a wind-drift factor.

3.3 Leeway coefficient

Floating objects on the ocean with a freeboard will not only move due to currents but will also have a motion directly linked to the direct wind forcing called the leeway (Breivik and Allen (2008), Breivik et al. (2013)). Finding the leeway coefficient to an object is typically done by a direct method from field measurements (Breivik et al., 2011). However, Sutherland et al. (2020) proposed a new way to calculate the leeway coefficient by interpolating model flow fields to the drifter positions. In this thesis, I use this new method to estimate the wind drift of the drifters deployed during the Kon-Tiki expedition.

For many objects at sea, it is necessary to include a leeward correction of the drift. The standard leeway model is given by

$$\mathbf{u}_d = \mathbf{u}_o + \boldsymbol{\alpha}\mathbf{U}_{10}, \tag{3}$$

where $\mathbf{u}_d$ is the drift vector, $\mathbf{u}_o$ is the ocean currents at the depth of the drifter, $\mathbf{U}_{10}$ is the 10-meter wind speed vector and $\boldsymbol{\alpha}$ is the implicit leeway factor. $\boldsymbol{\alpha}$ compensates for missing physics, for example, Stokes drift. However, it can be explicitly included if it is known. As the Stokes drift is becoming more available from wave prediction systems, Sutherland et al. (2020) defined a leeway model with the Stokes drift explicitly included

$$\mathbf{u}_d = \mathbf{u}_o + \mathbf{u}_s + \boldsymbol{\beta}\mathbf{U}_{10}, \tag{4}$$

Here $\mathbf{u}_s$ is the Stokes drift at the depth of the drifter and $\boldsymbol{\beta}$ is the leeway coefficient with Stokes drift explicitly included.

Typically the leeway coefficient is treated as a scalar with only an along-wind component. This scalar is used to parameterize a range of processes from direct wind drift to missing or unresolved physics. The leeway coefficient can also be a vector as a lot of objects also have a cross-wind component. Thus the new method suggests using an indirect approach to estimate the coefficients by interpolating the model fields to the objects' positions in time. The result is a time series of leeway coefficients that perfectly reproduce the drifter trajectory for a particular input of ocean currents, wind, and wave fields.

The ocean velocity and 10 m wind velocity are interpolated in space and time to the location of the drifter, using the function retrieve`wind_drift_factor` from OpenDrift.

$\boldsymbol{\alpha}$ contains all the uncertainties in the ocean and atmosphere models as well as the uncertainties in the drifter trajectories. The real part of $\boldsymbol{\alpha}$ will be in the along-wind component and the imaginary will be the crosswind direction, negative to the right of the wind direction. Comparing various drifters and forcing fields may provide

information about model uncertainty. Here $\boldsymbol{\alpha}$ and $\boldsymbol{\beta}$ are vectors allowed to vary in time and space. If model values are not biased then this provides the best estimate for $\boldsymbol{\alpha}$ and $\boldsymbol{\beta}$,

$$\boldsymbol{\alpha} = \frac{\mathbf{u}_d - \mathbf{u}_o}{\mathbf{U}_{10}} \tag{5}$$

$$\boldsymbol{\beta} = \frac{\mathbf{u}_d - \mathbf{u}_s - \mathbf{u}_o}{\mathbf{U}_{10}} \tag{6}$$

The velocity vectors are written in the complex form, $u + iv$, so that the real part, u, is positive to the east and that the imaginary part is positive to the north. This means that the real part of $\boldsymbol{\alpha}$ will be in the along-wind direction and the imaginary part will be in the cross-wind direction (negative to the right of the wind direction).

3.4 Simulations

3.4.1 Reproducing Drifter Trajectories with OpenDrift

This section describes the simulations conducted to assess how well ORAS5, ERA5, and OpenDrift reproduce the observed drifter trajectories from the Kon-Tiki 2 expedition before and after they lost their drogue. All the drifter time series were split into two, before and after the drogue was lost. Two seedings of 100 particles each were performed for the drifters with their drogue still attached. The particles were seeded randomly within a radius of 50 km of the deployment position. One set of particles was forced with the current at 16 meters depth, which was the closest depth to 15 meters in ORAS5. The second seeding was forced with the surface currents. The duration of the simulation was from the deployment time until the time the drifter lost its drogue or stopped transmitting. For the drifters without their drogue, three similar seedings were done, except now they were seeded randomly 50 km within a radius of the position the drifter lost its drogue. The first seeding was forced with only the surface currents, the second with a combination of surface currents and Stokes drift, and the third with the surface currents with an additional wind drift factor. The simulation was then run from the date it lost its drogue until the drifter stopped transmitting.

3.4.2 Long term simulations of marine plastic debris

This section describes the two different experiments to simulate plastic drift. The first one was to simulate the drift of microplastic, and the second was to simulate the drift of macroplastic. The definition for the size of microplastic is not generally agreed-upon, some define it as smaller than 5 mm and others smaller than 1mm (Law, 2017). Therefore, we chose microplastic to have the same properties as a passive tracer at the surface, meaning that it follows the surface current. Macroplastic normally refers to particles larger than microplastic, so for the macroplastic case, I gave the particles a wind drift factor of 1% based on the estimated leeway coefficient for the undrogued SVP drifters. For both the microplastic and macroplastic simulations, a total of 165252 particles were seeded, corresponding to one particle per grid point in the domain.

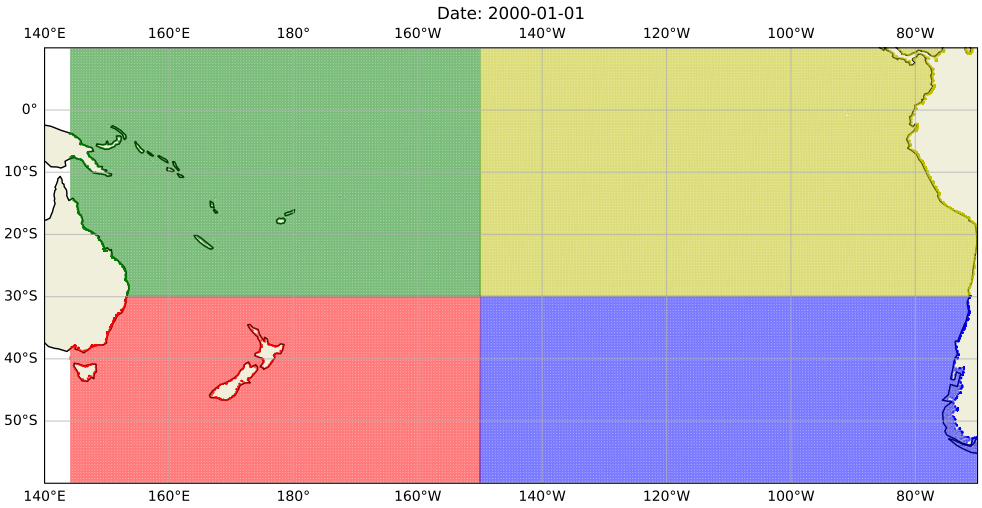

Figure 5: The first time step of the plastic simulations, showing the start distribution of particles. The colors indicate the seeding region, NW (green), SW (red), SE (blue), and NE (yellow).

For the simulations, a virtual particle was seeded in each grid point of the ORAS5 data set. In order to keep track of where the particles originated from, the domain was split into four different sections; North-East (NE), North-West (NW), South-East(SE), and South-West (SW) (Figure 5). A definition of the regions is found in Table 2. Furthermore, the simulation was run for 20 years, from 01-01-2000 to 31-12-2019, with weekly outputs. Both simulations were forced with the surface currents from ORAS5, but the macroplastic simulation was also forced with wind fields from ERA5. For the simulation of drift of microplastic and macroplastic in the South Pacific gyre, without knowing where the sources of plastic are, experiments, where all the particles were seeded at the same time in a uniform grid, were conducted. In order to reduce the memory use and run-time, the four different regions were run separately but had the same starting times and duration. If a grid point is located on land, it is moved to the closest ocean grid point. This might result in some ocean grid points contains more than one particle. If the virtual particle "washes onshore", the particle becomes marked as stranded and deactivated. The particle also becomes deactivated if it hits the domain boundaries at 10°N, 60°S, 140°E and 70°W.

Table 2: Definiton of seeding regions and the number of particles within the region

	Longitude min	Longitude max	Latitude min	Latitude max	Number of particles
NE	150 °W	70°W	30°S	10°N	51681
NW	144°E	150 °W	30°S	10°N	42665
SE	150°W	70°W	60°S	30°S	38841
SW	144 °E	150 °W	60°S	30°S	32065

4 Results

4.1 Assessment of ORAS5

The observed drifter trajectories together with the virtual particles forced with surface currents and the 16-meter depth currents were used to assess how well ORAS5 predicts the observed drifter trajectories. Drifter 139562 is shown in Figure 6 and the trajectory maps for the remaining drifters are shown in Appendix A.1. The yellow star marks the deployment position of the drifter and the center of the seeding area for the virtual particles. By visual inspection of the trajectories, both the surface current and 16-meter current do an adequate job at reproducing the observed trajectory, both when it comes to pattern and length. It is not obvious if the surface current or the 16-meter depth current best matches the observed trajectories.

The 2D histogram for the leeway coefficient $\boldsymbol{\alpha}$ for the drogued drifter 139562 (Figure 7) shows that the along wind component of $\boldsymbol{\alpha}$ is zero and the cross-wind is less than 1%. Averaging across all the drouged drifters shows that the mean is less than 1% for both the along- and cross-wind component, thus the wind effects on the drogued drifter are minimal. The 2D histograms for the remaining drifters are found in Appendix A.3.1.

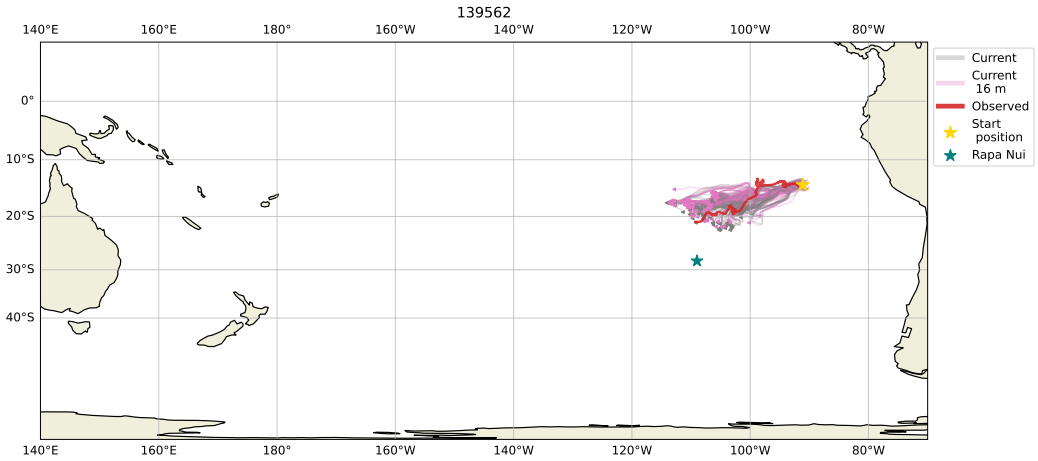

Figure 6: The observed trajectory of drifter 139562 (red), the virtual drifters forced with only the surface currents (grey), and the virtual drifters forced with currents from a depth of 16 meters (pink). The triangles mark the end positions of the virtual particles. The yellow star indicates the deployment position of the drifter and the seeding point for the virtual drifters. The teal star marks the position of the island Rapa Nui.

The observed trajectories for 3 drogueless drifters and the virtual particles forced with various forcing are shown in Figure 8, the rest of the drifters is shown in Appendix A.2. The observed trajectory is the red thick line, the blue lines are the surface current with Stokes drift, the grey are the surface current and the orange are the surface current with the inclusion of the leeway factor in the along wind direction estimate for the specific drifter. The triangles indicate the end positions of the simulated drifters. For all three of the drifters, the inclusion of Stokes drift gives the drifter a too strong northwards movement at the beginning pushing the virtual drifters into the equatorial current system, thus the total displacement of these particles is too large compared

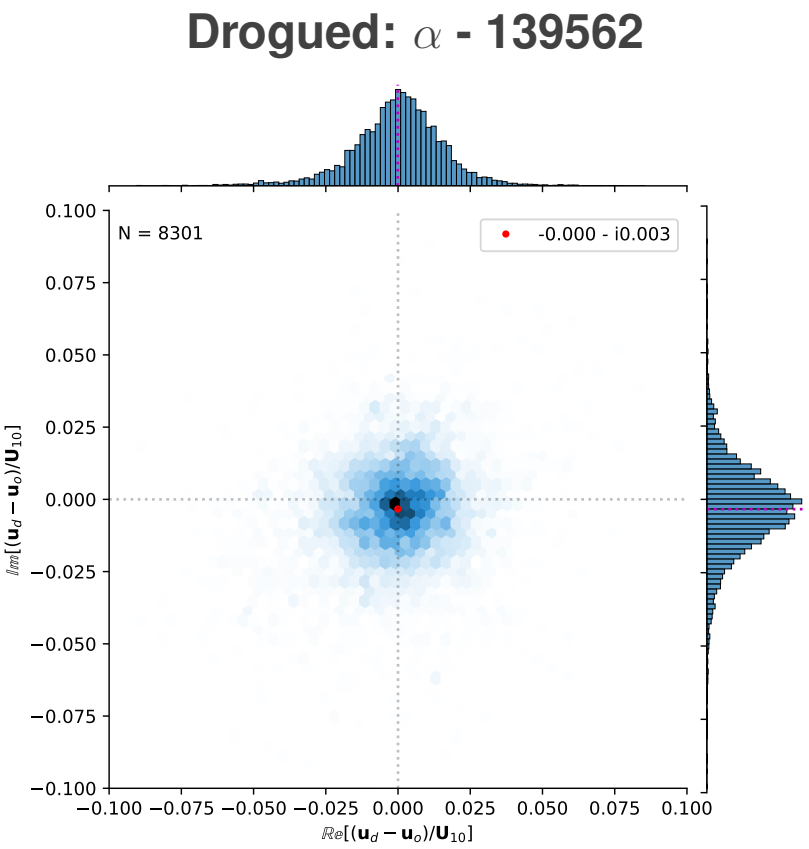

Figure 7: 2D histogram of the leeway coefficient, α (implicit Stokes drift), and the corresponding 1D histograms for the along-wind and cross-wind components for drifter 139562, with the drogue, forced with the currents at 16 meters depth from ORAS5 and winds from ERA5. The red dot and lines indicate the mean. Figure provided by Graig Sutherland.

to the observed drifter path. The virtual drifters forced with only the surface currents seem to vaguely match the observed trajectory for drifter 139800 (Figure 8c). For drifters 139908 and 139563 (Figure 8a & 8b) the observed drifter seems to follow a path between the current and the current with Stokes drift trajectories, thus implying that there is a different forcing in play. The trajectories forced with the surface currents and the calculated leeway factor provide a better fit both in direction and distance traveled over the period.

How well the simulated trajectories resemble the observed trajectories varies in the data set. But for drifter 139800 (Figure 8c) both the current and wind drift simulation perform relatively well. The current in combination of wind simulation matches better in length, which is expected as it is forced with the estimated leeway coefficient.

For drifter 139008 (Figure 8a) the simulated drifters only forced with the surface currents go to the east of the observed trajectory, the Stokes drift combination goes too far north and the wind-forced drifter goes too far west before they start going south and east again. For this drifter, all of the different forcings place the simulated drifters into different current systems. The one forced with winds in addition to the surface currents provides the best match out of the three, at least at the beginning of the simulation. None of the forcings manages to reproduce the eddying motion of the drifter.

It appears as the drifter simulations with the leeway coefficients, and also the surface currents perform better when the observed drifters travel southward rather than westward at around 20°S.

To estimate the wind effects on the drifters, the leeway coefficient, $\boldsymbol{\alpha}$ and $\boldsymbol{\beta}$ were calculated, and the resulting 2D histograms of the time series for drifter 139562 are shown in Figure 9, and the rest in Appendix A.3.2. The virtual drifters in Figure 8 are forced with the surface current and the mean leeway coefficient $\boldsymbol{\alpha}$ is estimated for the particular undrogued drifter. Both $\boldsymbol{\alpha}$ and $\boldsymbol{\beta}$ range from 0.5% to 2.2% and the results do not appear sensitive to Stokes drift.

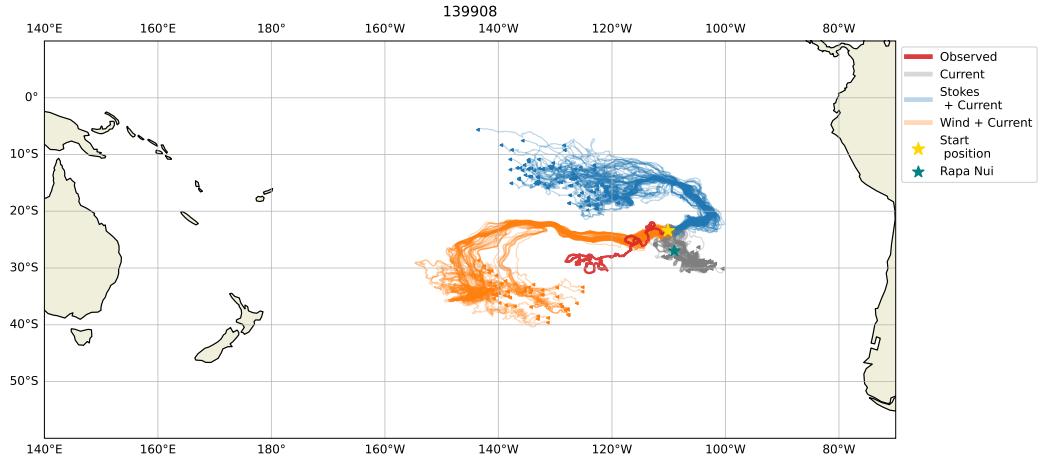

(a)

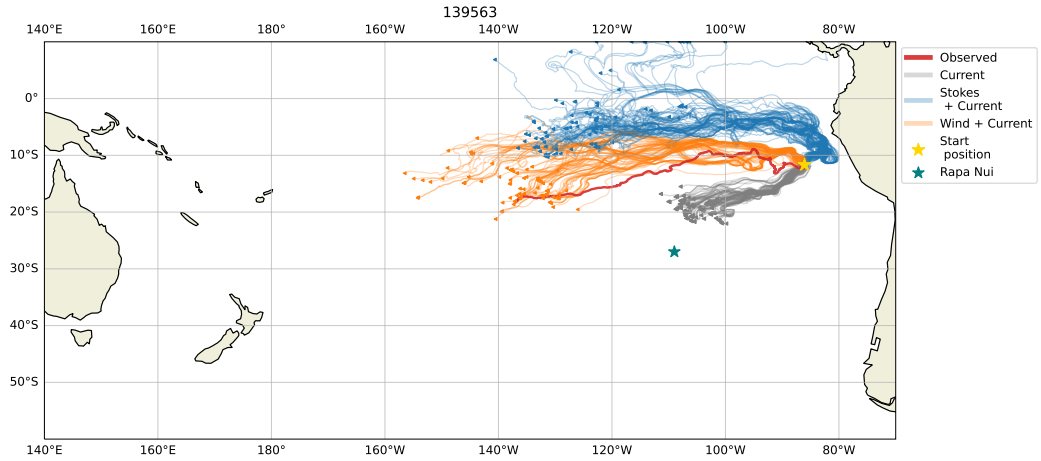

(b)

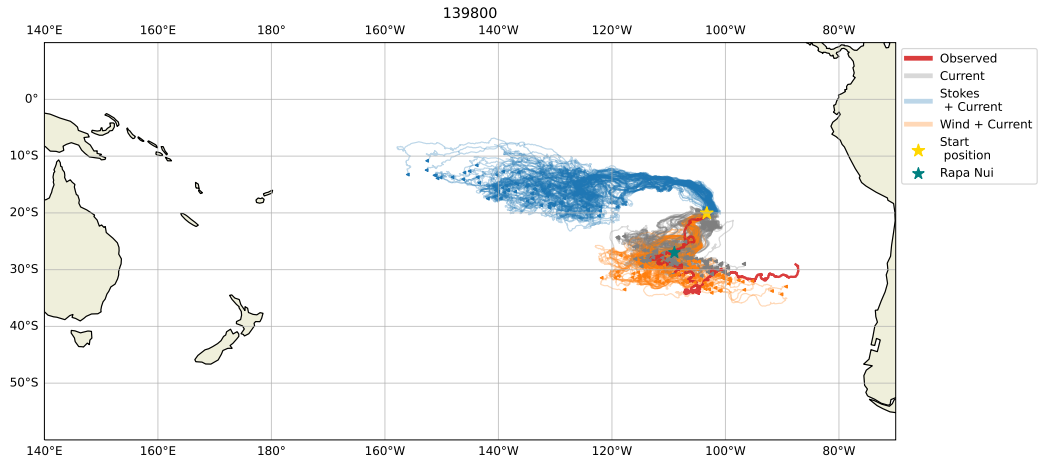

(c)

Figure 8: The observed trajectory (red) for the undrogued drifters, the virtual drifters forced with only the surface currents (grey), the virtual drifters forced with a combination of Stokes drift and surface currents (blue) and the virtual drifters forced with surface currents and wind. The triangles mark the end positions of the virtual particles. The yellow star indicates the deployment position of the drifter and the seeding point for the virtual drifters. The teal star marks the position of the island Rapa Nui.

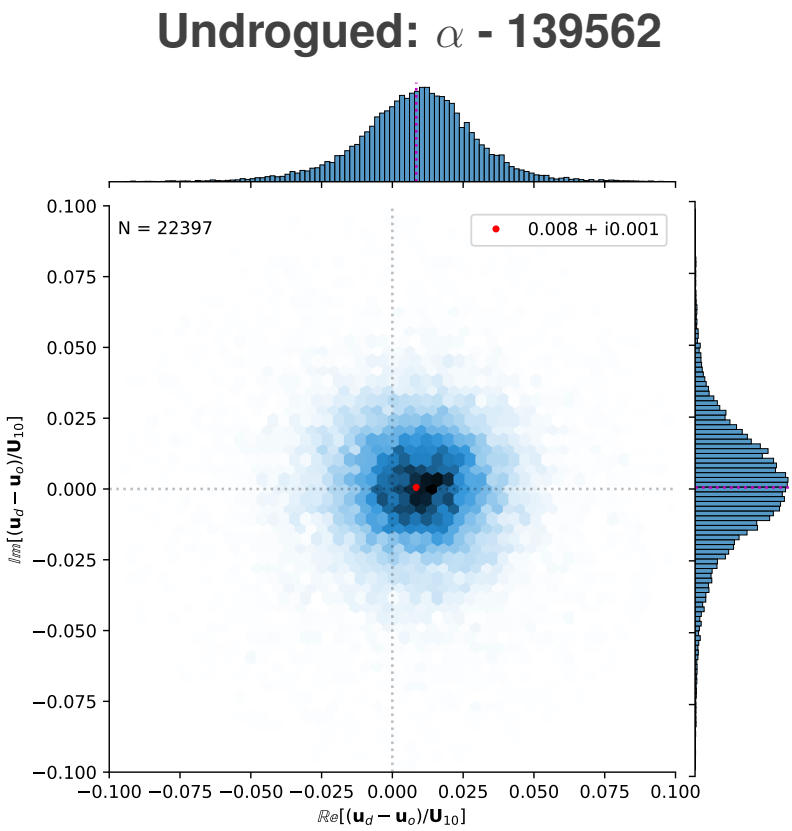

(a)

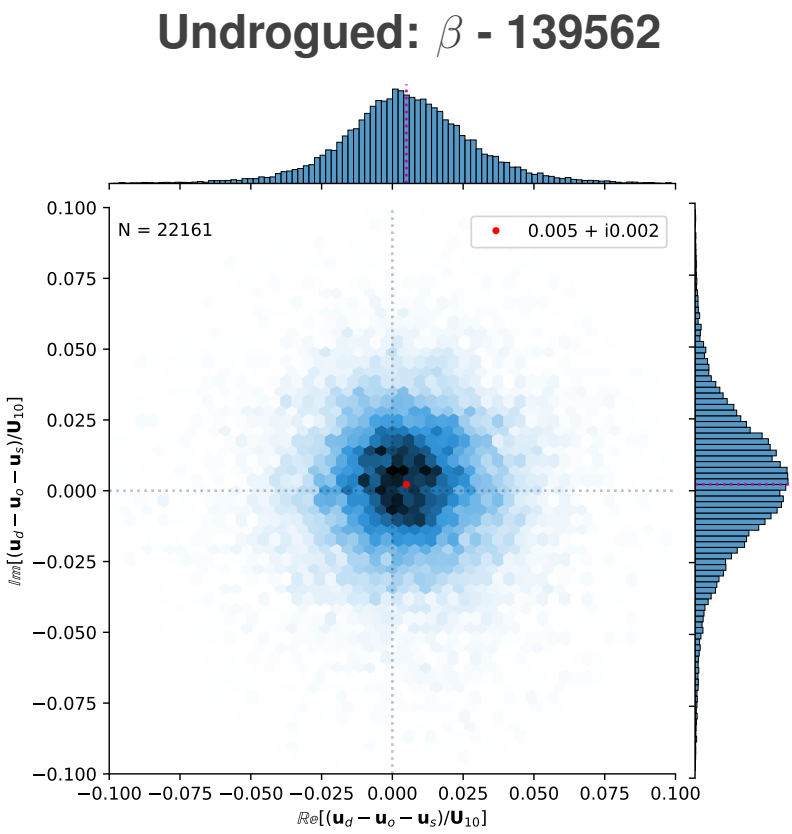

(b)

Figure 9: 2D histograms of the leeway coefficients and the corresponding histograms for the along-wind and cross-wind components for drifter 139562 after drogue is lost. (a) α forced with surface currents from ORAS5 and winds from ERA5. (b) β with the Stokes drift explicitly included from ERA5. Figures provided by Graig Sutherland.

4.2 Long term simulations of marine plastic debris

4.2.1 Microplastic

Figure 10 summarizes the microplastic drift from January 2000 to December 2019. Full animation of the experiment can be found here: `https://vimeo.com/722524481`. The simulation was initiated by seeding a uniform grid with a resolution of 0.25°, corresponding to 165252 particles, and forced with the surface currents from ORAS5. The particles seeded in the four different regions have separate colors to keep track of their origin and pathway. Within the first year, the equatorial region is almost cleared from particles. After five years, the particles gathered in a belt between 20 and 45°S. After ten years, the belt is still present though narrower, and a large quantity of the particles accumulated around 30°S and 90 °W. At the beginning of 2015, the accumulation zone became more defined, and at the end of the simulation, this belt remains as a faint trail of particles.

Figure 11 shows the percentage of particles in each region and particles that exit the domain or get stranded over time. Twelve years into the simulation, 57 % of the particles are in the eastern domain. In the western part of the domain, the density of particles increases slightly before the particles are transported eastward. The eastern domain reaches the maximum distribution after 12 years, where the remaining particles fluctuate between NE and SE. After four years around 20 % of all the particles stranded and 20 % exited the South Pacific. The stack plots in Figure 13 shows how the microplastic move over the course of the simulations. The particles seeded in NW use about four years to reach the eastern part and over 60% of the particles in this region strand or cross the boundaries of the South Pacific. For the SW region, less than 10 % of the particles exit the domain. After 8 years, most of the particles are in the eastern part of the South Pacific. For the particles seeded in the NE region, 20% of the particles are lost, mostly over the equator, and approximately 25% strands. Of the SE particles around 20 % of the particles exit the domain and 15 % strands. Four years into the simulation the particles oscillate between the NE and SE, with most of the particles in the NE region. The map in Figure 12 shows the distribution of the particles in the last time step. The maximum is at 28°S and 86 °W. The particles accumulated for the most part between 100-85 °W and 25-35 °S.

As a first step to investigate any potential influences of ENSO on the distribution of the microplastic I calculated the correlation between the fraction of microplastic located in the SE quadrant and lagged values of the Niño 3.4 index (Figure 14). As the Niño 3.4 index is a monthly value, the fraction from the simulation is averaged over the same month. I am using the simulated fraction period from 2011 to 2019, excluding the early transitional period and focusing on the period where the total number of particles in the eastern accumulation zone is relatively constant.

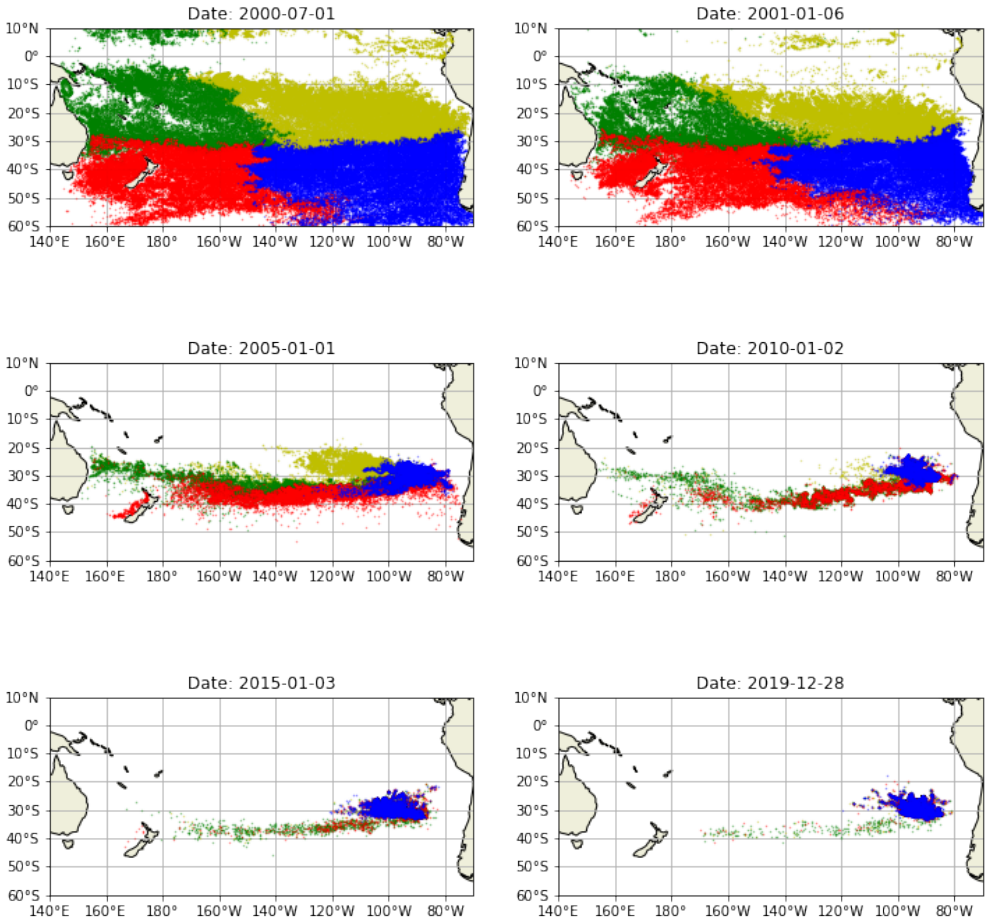

Figure 10: The time evolution of the microplastic accumulation zone for selected time steps between 01-07-2000 and 28-12-2019. The colors indicate the origin of the particles. Note: the blue color is plotted last, hence the accumulation of in the final time steps appears blue.

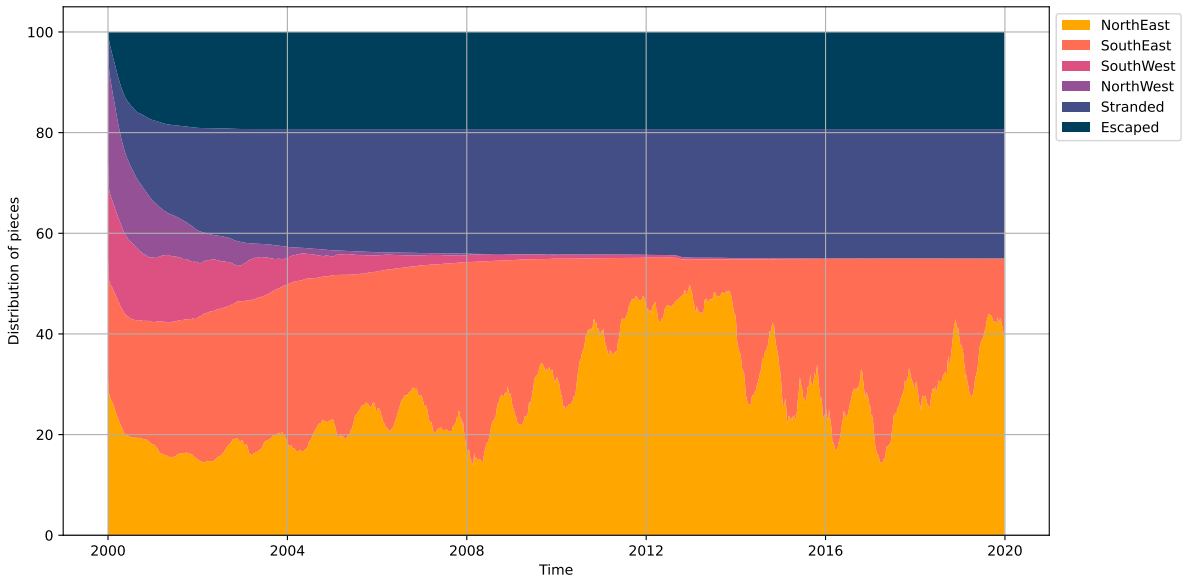

Figure 11: Distribution of the virtual microplastic particles over time. The colors indicate the percentage of the total amount of particles contained within each of the four seeding regions, North East (yellow), South East (orange), South West (pink) and North West (purple) as well as the percentage of particles that have stranded (violet) or left the model domain (indigo).

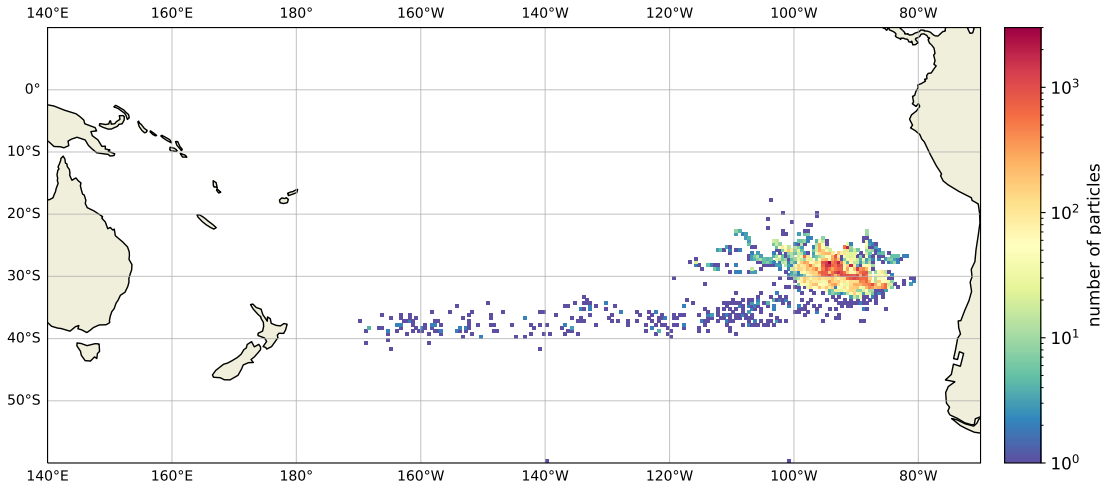

Figure 12: Number of particles per 0.5°in the final time step of the microplastic simulation.

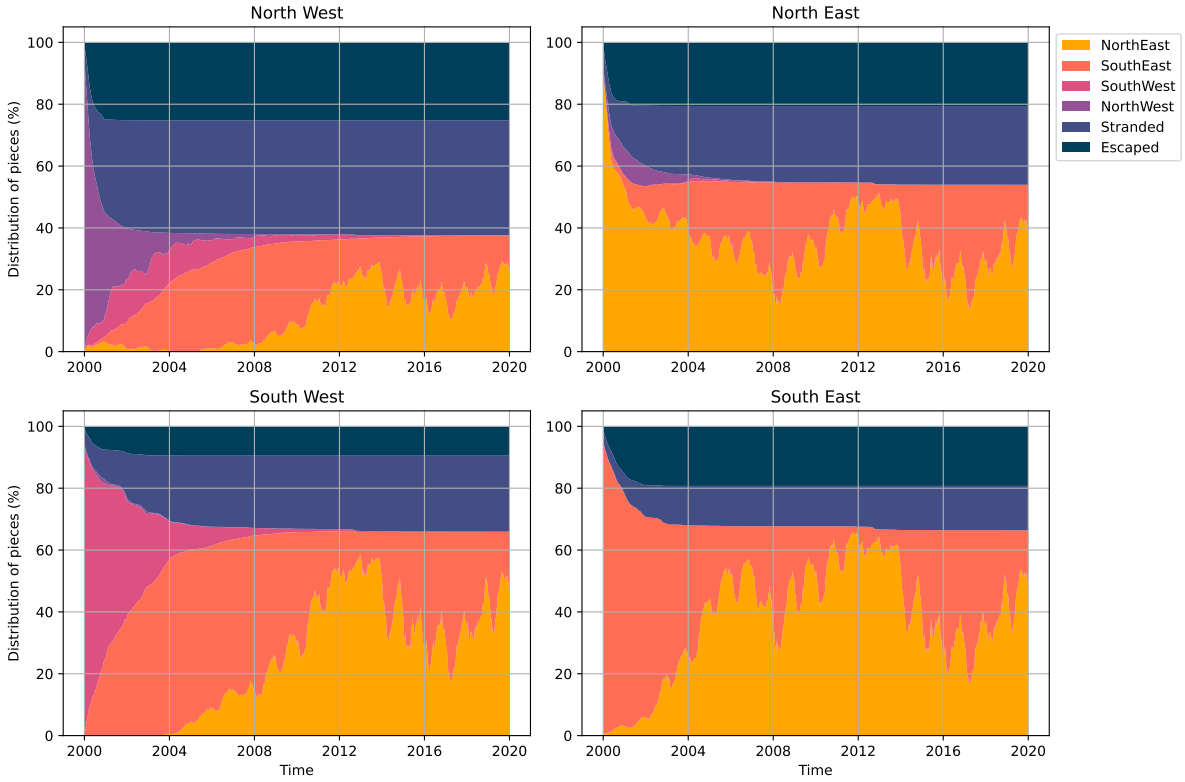

Figure 13: Distribution of the microplastic particles over time based on the region it was seeded in. The colors indicate the percentage of particles within a region.

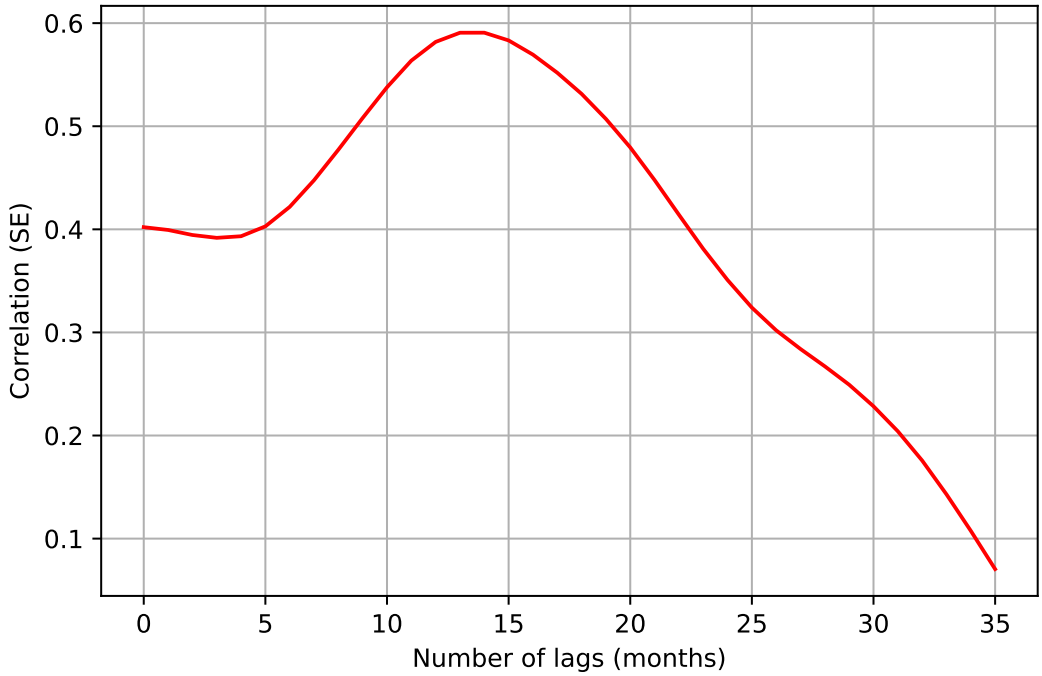

Figure 14: Correlation between the fraction of particles in the SE quadrant and lagged Niño 3.4 index in the period 2011 to 2019.

4.2.2 Macroplastic

The simulation for the 165252 uniformly seeded macroplastic particles with a 1% leeway factor is summarized in Figure 15. The animation of the complete run can be found here: `https://vimeo.com/722449217`. The different colors denote the different seeding regions. Within the first six months, the equatorial region is cleared of plastic. After a year, most plastic north of 10°S is also cleared of particles except for some particles outside Panama/Colombia. Within five years, the particles have gathered in a pretty large belt between 20 and 40°S, and an accumulation zone formed at 120-80°W and 20-35°S. In the last four years of the simulation, we see that the particles become more accumulated with very few particles left west of 130°W.

The evolution of the macroplastic distribution over time (Figure 16) exhibits a rapid accumulation in the eastern part of the Southern Pacific. After the first two years, 20 % of the particles escape the South Pacific by crossing the equator, going through the Drake Passage, or going too far South into the Antarctic Circumpolar Current. It only takes two years before hardly any more particles escape. After four years, almost 40 % of the particles are marked as stranded. For the last 16 years of the simulations, almost all of the particles left are in the eastern domain, but they change between being south and north of the 30°S line.

Figure 17 illustrates the density of microplastic at the final time step in the solution with the number of particles per 0.5 °. There are higher concentrations of particles just south of 30°S and 100°W. The plastic is spread out on a large area, from 85 to 125°W, and some particles sparsely spread to New Zealand.

The stack plots for each seeding region (Figure 18) show how the particles behave during the simulation. For the western regions, it only takes two years before the particles reach the eastern part. During those two years, 45 % of the NW particles strands. The NW region is the one that contributes least to the end concentration of plastic. For the particles seeded in the NE, some take a detour into the NW region. About 40% of the NE particles strands and around 38 % are left at the end of the run. We see the same variability in these plots as we did in the complete run, with the remaining particles crossing between the NE and SE (30 °S).

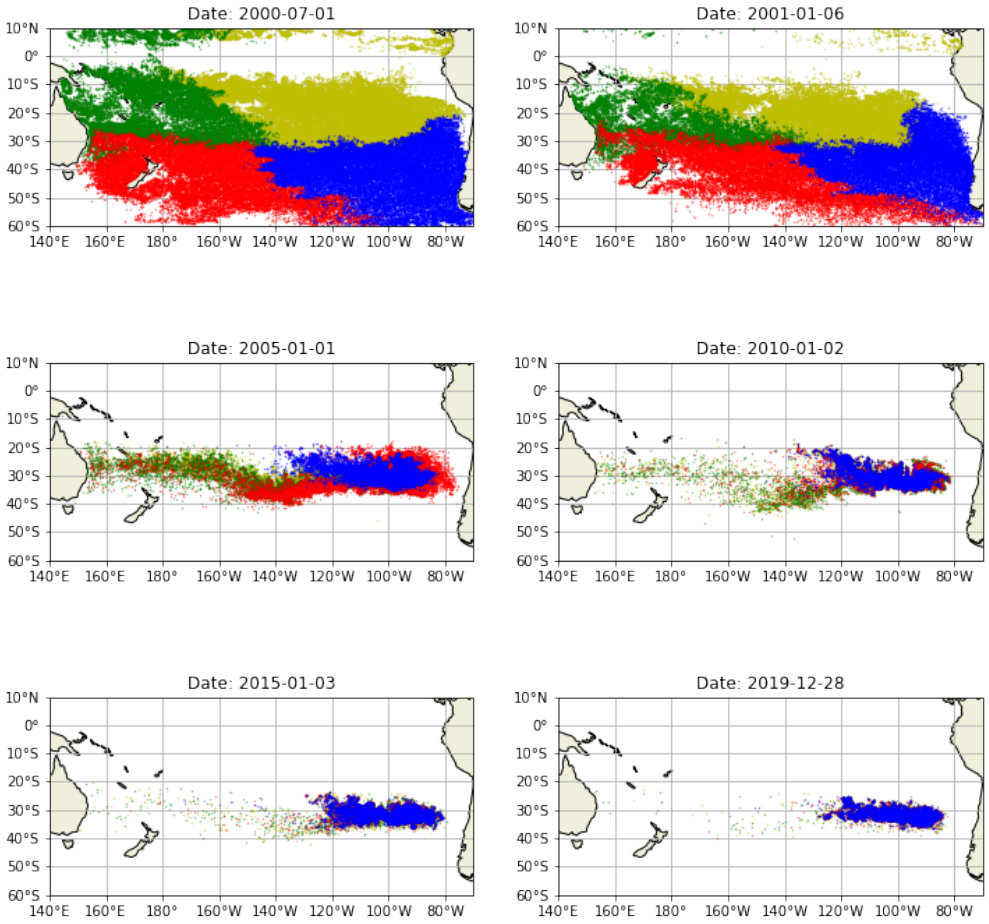

Figure 15: The time evolution of the macroplastic accumulation zone for selected time steps between 01-07-2000 and 28-12-2019. The colors indicate the origin of the particles. Note: the blue color is plotted last, hence the accumulation of in the final time steps appears blue.

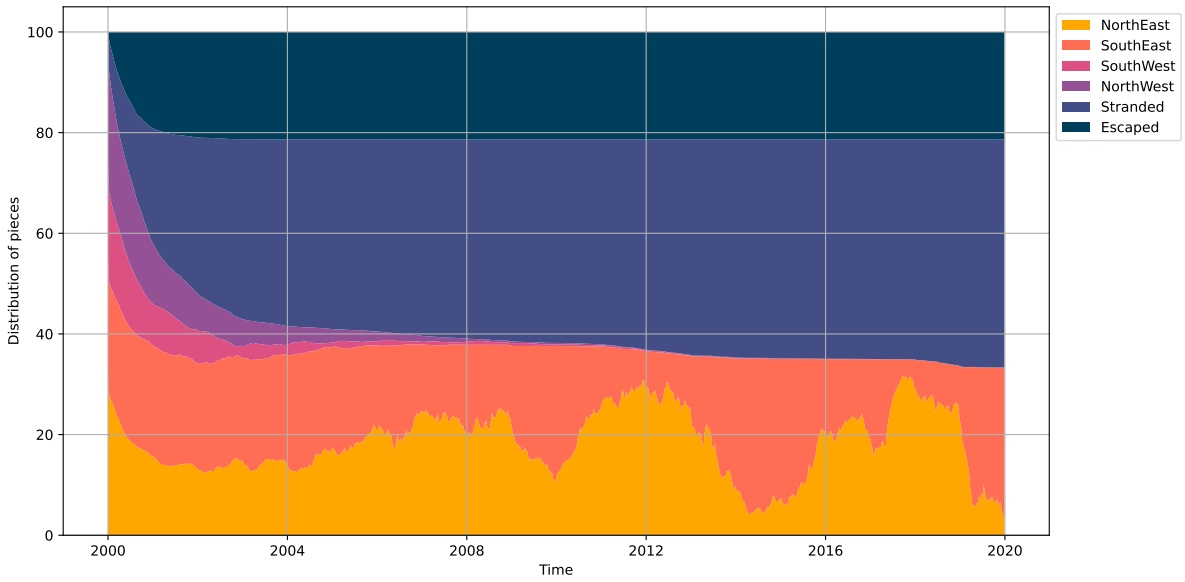

Figure 16: Distribution of the virtual macroplastic particles over time. The colors indicate the percentage of the total amount of particles contained within each of the four seeding regions, North East (yellow), South East (orange), South West (pink), and North West (purple) as well as the percentage of particles that have stranded (violet) or left the model domain (indigo).

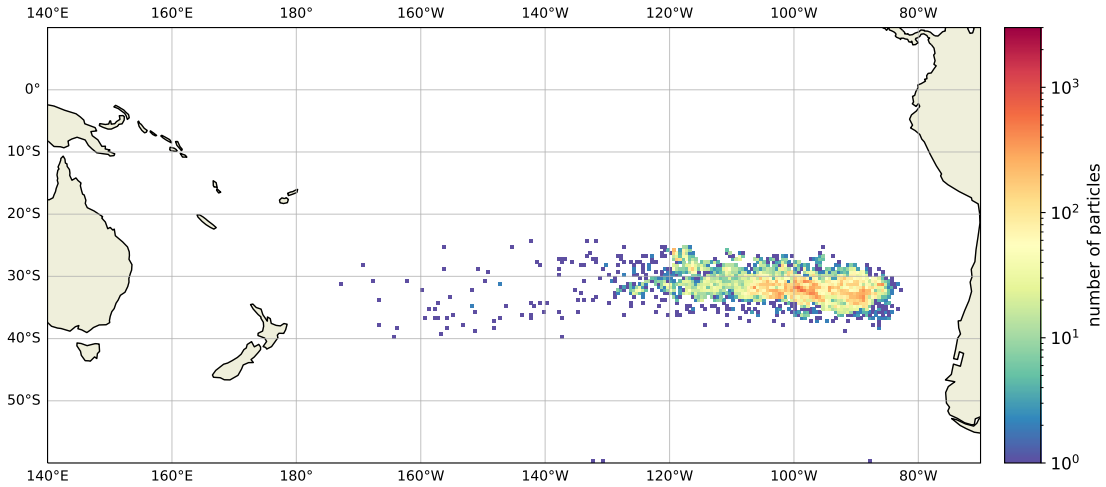

Figure 17: Number of particles per 0.5 °in the final time step (2019) of the macroplastic simulation.

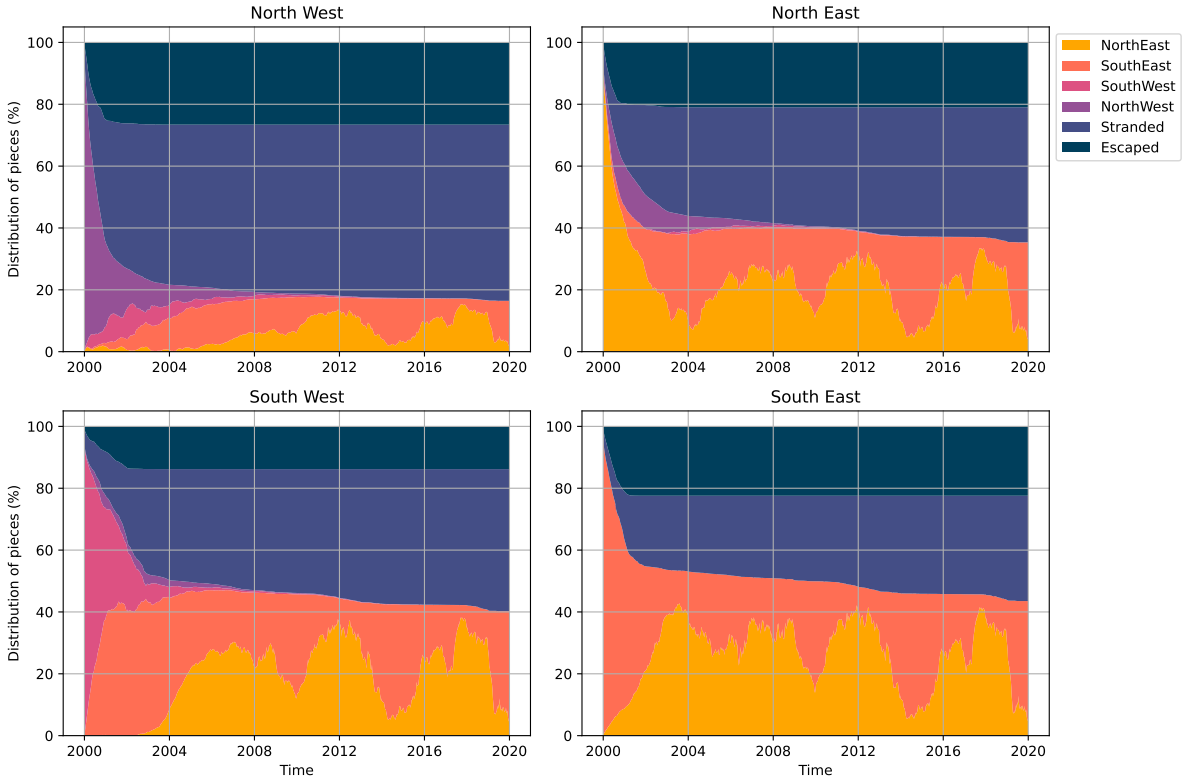

Figure 18: Distribution of the macroplastic particles over time based on the region they were seeded in. The colors indicate theregions.

5 Discussion

5.1 Drifters

In order to assess if the ocean reanalysis ORAS5 could be used for studying the drift of marine plastic debris in the ocean, two experiments were done by comparing observed trajectories with simulated trajectories for drogued and undrogued drifters. ORAS5 did a varying job in reproducing the undrogued drifters but a better job reproducing the drogued. This result was as expected because no wind was included in those simulations as the leeway coefficient was estimated to be less than 1%. These results are consistent with the design of SVP drifters as they are designed to have minimal wind drift Lumpkin et al. (2017). Sutherland et al. (2020) also found comparable values when they studied the wind effect on the SVP drifters. By visual inspection, it is hard to determine whether it is the surface currents or the currents at 16-meter that provide the best fit for the drogued drifters. A reason may be that the vertical resolution for the currents may be too coarse in ORAS5. Nevertheless, ORAS5 satisfactorily models the drift of the drogued SVP drifter.

For the undrogued drifters, just using the surface currents underestimates the length of the distance the observed drifter travels. The inclusion of Stokes drift seems to push the virtual particles too far north and into a westward flowing current system. Including only the along-wind component of the estimated leeway coefficient seems to produce a much better fit concerning the direction and distance between the simulated and observed trajectories. Therefore, it appears reasonable to use ORAS5 surface currents together with the wind fields from ERA5 with a 1% wind drift factor to simulate macro plastic.

The leeway coefficients for the undrogued drifters were estimated using a new indirect method (Sutherland et al., 2020). The along-wind leeway coefficients were found to be a range of values between 0.5 and 2.2% and the cross-wind leeway coefficients were less than 1% for both the implicit and explicit leeway model. These values are comparable to Poulain et al. (2009), which found that the wind drift of undrogued SVP drifters is approximately 2%. The drifters that are on the lower end of the range may have some additional drag if the drogue still has some parts of the drogue attached.

5.2 Plastic Drift

This thesis investigates plastic's behavior and residence times in the South Pacific gyre. Using Lagrangian particle tracking with ocean and atmospheric forcing from reanalysis products, I find that microplastic and macroplastic accumulates in the eastern part of the South Pacific and forms a well-defined plastic gyre within 12 years. By looking at both microplastic and macroplastic, we can gain a better understanding of how the winds influence the accumulation process. The findings suggest that both microplastics and macroplastics accumulate in the same general area of the eastern South Pacific, between 120-80°W and 20-40°S. The location of these zones is consistent with the observations (Eriksen et al., 2013) and simulations (Maximenko et al. (2012), Maximenko et al. (2012), Martinez et al. (2009), Onink et al. (2019)). Performing the experiments a second time, but starting the simulation five years later in 2005, yielded similar results

(not shown in this thesis). After the plastic reaches the accumulation zone in the east, the zone and borders are not stationary in time but vary in shape and location. However, the number of plastic particles within the zones are relatively steady, indicating that there is no, or minimal, leakage of plastic over the final 12 years of simulation. Martinez et al. (2009) also looked at the leakiness of the plastic accumulation zone but with an 8-year simulation and concluded that the floating marine debris could not leave the region anymore. However, it is suggested that material could escape the region in models with sufficient horizontal resolution in which small-scale structures can modify the mean current (Maes et al., 2016). When comparing the micro and macro simulation, more plastic strands during the macro simulation than the micro simulation—resulting in fewer particles in the macro gyre than in the microplastic gyre. The stranding in the microplastic simulation is arguably artificial as particles cannot cross onto land without winds and/or waves. The macro gyre is also spread over a larger area than the microplastic. By studying the final twelve years of experiments, the macro gyre appears to have a circular motion on a faster time scale than the micro. This is probably due to the variability in the winds. Surprisingly, the seasonal variation of the particles crossing the 30°S line is more prominent in the micro than the macro simulation. This is likely a result of the macroplastic accumulation zone/plastic gyre having its highest concentration of particles further south than the microplastic accumulation zone. The 30 °S line goes through the part of the microplastic gyre. Thus more particles can cross this line. On top of the seasonal variability, there seems to be a signal on a longer time scale, which might be an ENSO signal. The contemporary correlation between the Niño 3.4 Index and the fraction of particles in the SE region (Figure 14) is about 0.4 for the first five months and then increases to close to 0.6 after 12 months and declines steadily towards zero after that. This indicates that the presence of ENSO events exerts some influence on the location of the simulated microplastic accumulation zone. Periods with a large Niño-index value slowly pull the patch northwards, while low values push the plastic gyre southwards. However, this is just a first step to see if there is an ENSO signal and the correlation is calculated with the crossing of an arbitrary line, therefore further investigation would be needed, but this is beyond the scope of this study. In the experiments for modeling the transport of floating marine debris, I seeded a uniform grid over the entire basin as a one-time seeding. It is highly unrealistic that such an amount of plastic is released at the same time. However, as the input distribution and mass budget of marine plastic is highly uncertain (Hardesty et al. (2017) Lebreton et al. (2017)), and the purpose of this thesis was to examine the residence times of plastic in the South Pacific Gyre, I assumed that the effect of the initial distribution was small. The studies by (Van Sebille et al. (2012), Maximenko et al. (2012) Lebreton et al. (2012)) corroborates this assumptions. For the macro simulation, the added wind-drift factor was only added in the along-wind direction because the estimated leeway coefficients for the cross-wind component were less than 1%. Thus the macroplastic has approximately the same wind drift as the undrogued drifters, meaning that it would have similar shapes and sizes as the undrogued drifters. The understanding of plastic movements in the marine environment would significantly improve by models including wind and wave effects, fragmentation processes, biofouling, and using a plethora of particles and items of different shapes and sizes.

6 Conclusion

In this thesis, I used the open-source Lagrangian particle tracking framework OpenDrift to reproduce observed drifter trajectories and simulate the large-scale drift of marine plastic in the South Pacific subtropical gyre. I conducted three different simulations. First, I used simulations to see how well the ORAS5, ERA5, and OpenDrift reproduced the observed drifter trajectories from the Kon-Tiki 2 expedition before, and after, they lost their drogue, and until they stopped transmitting. The results showed that ORAS5 did a varying job in reproducing the undrogued drifters, but a better job at reproducing the trajectory of the drogued drifters. This result was as expected as no wind effects were included in those simulations as the leeway coefficient was estimated to be less than 1%.

The two other experiments simulates the behavior of microplastic and macroplastic, respectively, where microplastic is defined as passive tracers which follows the surface currents and macroplastic is defined as floating particles with 1% leeway over a period of 20 years from 2000 to the end 2019. From the simulations of the drift of micro- and macroplastic using Lagrangian particle tracking with ocean and atmospheric forcing from reanalysis products, I found that microplastic and macroplastic accumulates in the eastern part of the South Pacific and forms a well-defined plastic gyre within 12 years. After the plastic reaches the accumulation zone, the zone and borders are not stationary in time but vary in shape and location. However, the number of plastic particles within the zones are relatively steady, indicating that there is no, or only minimal, leakage of plastic over the final years of simulation. The seasonal variation of the particles crossing the 30°S line is more prominent in the micro than the macro simulation. On top of the seasonal variability, there seems to be a signal on a longer time scale, which might be an ENSO signal, but this would need further investigation. With this improved knowledge of the trajectories of plastic litter and how natural variability affects this, we can initiate plans for better look for their sources with an aim of cleaning up the sources of plastic and reducing or eliminating them in the future.

References

A. L. Andrady. Microplastics in the marine environment. *Marine Pollution Bulletin*, 62 (8):1596–1605, 8 2011. ISSN 0025-326X. doi: 10.1016/J.MARPOLBUL.2011.05.030.

A. Bennett. *Lagrangian Fluid Dynamics*. Cambridge University Press, 3 2006. ISBN 9780521853101. doi: 10.1017/CBO9780511734939. URL https://www.cambridge.org/core/product/identifier/9780511734939/type/book.

P. Berrisford, D. Dee, K. Fielding, M. Fuentes, P. Kallberg, S. Kobayashi, and S. Uppala. The ERA-Interim Archive. 2009. URL http://www.ecmwf.int/publications/library/do/references/list/782009%5Cnhttp://centaur.reading.ac.uk/1997/.

Ø. Breivik and A. A. Allen. An operational search and rescue model for the Norwegian Sea and the North Sea. *Journal of Marine Systems*, 69(1-2):99–113, 1 2008. ISSN 0924-7963. doi: 10.1016/J.JMARSYS.2007.02.010.

Ø. Breivik, A. A. Allen, C. Maisondieu, and J. C. Roth. Wind-induced drift of objects at sea: The leeway field method. *Applied Ocean Research*, 33(2):100–109, 4 2011. ISSN 0141-1187. doi: 10.1016/J.APOR.2011.01.005.

Ø. Breivik, A. A. Allen, C. Maisondieu, and M. Olagnon. Advances in search and rescue at sea. *Ocean Dynamics*, 63:83–88, 2013. doi: 10.1007/s10236-012-0581-1.

A. Cózar, F. Echevarría, J. I. González-Gordillo, X. Irigoien, B. Ibeda, S. Hernández-León, A. T. Palma, S. Navarro, J. García-de Lomas, A. Ruiz, M. L. Fernández-de Puelles, and C. M. Duarte. Plastic debris in the open ocean. *Proceedings of the National Academy of Sciences of the United States of America*, 111(28):10239–10244, 7 2014. ISSN 10916490. doi: 10.1073/pnas.1314705111.

K.-F. Dagestad, J. Röhrs, Ø. Breivik, and B. Ådlandsvik. OpenDrift v1.0: a generic framework for trajectory modelling. *Geoscientific Model Development*, 11 (4):1405–1420, 4 2018. ISSN 1991-9603. doi: 10.5194/gmd-11-1405-2018. URL https://gmd.copernicus.org/articles/11/1405/2018/.

A. Dawson. Windspharm: A High-Level Library for Global Wind Field Computations Using Spherical Harmonics. *Journal of Open Research Software*, 4(1):31, 8 2016. doi: 10.5334/jors.129.

S. Elipot, R. Lumpkin, R. C. Perez, J. M. Lilly, J. J. Early, and A. M. Sykulski. A global surface drifter data set at hourly resolution. *Journal of Geophysical Research: Oceans*, 121(5):2937–2966, 5 2016. ISSN 21699291. doi: 10.1002/2016JC011716.

M. Eriksen, N. Maximenko, M. Thiel, A. Cummins, G. Lattin, S. Wilson, J. Hafner, A. Zellers, and S. Rifman. Plastic pollution in the South Pacific subtropical gyre. *Marine Pollution Bulletin*, 68(1-2):71–76, 2013. ISSN 0025326X. doi: 10.1016/j.marpolbul.2012.12.021. URL http://dx.doi.org/10.1016/j.marpolbul.2012.12.021.

M. Eriksen, L. C. M. Lebreton, H. S. Carson, M. Thiel, C. J. Moore, J. C. Borerro, F. Galgani, P. G. Ryan, and J. Reisser. Plastic Pollution in the World's Oceans: More than 5 Trillion Plastic Pieces Weighing over 250,000 Tons Afloat at Sea. *PLoS ONE*,

2014. doi: 10.1371/journal.pone.0111913. URL https://doi.org/10.1371/journal.pone.0111913.

B. D. Hardesty, T. J. Lawson, T. van der Velde, M. Lansdell, and C. Wilcox. Estimating quantities and sources of marine debris at a continental scale. *Frontiers in Ecology and the Environment*, 15(1):18–25, 2 2017. ISSN 15409309. doi: 10.1002/fee.1447.

H. Hersbach, B. Bell, P. Berrisford, S. Hirahara, A. Horányi, J. Muñoz-Sabater, J. Nicolas, C. Peubey, R. Radu, D. Schepers, A. Simmons, C. Soci, S. Abdalla, X. Abellan, G. Balsamo, P. Bechtold, G. Biavati, J. Bidlot, M. Bonavita, G. De Chiara, P. Dahlgren, D. Dee, M. Diamantakis, R. Dragani, J. Flemming, R. Forbes, M. Fuentes, A. Geer, L. Haimberger, S. Healy, R. J. Hogan, E. Hólm, M. Janisková, S. Keeley, P. Laloyaux, P. Lopez, C. Lupu, G. Radnoti, P. de Rosnay, I. Rozum, F. Vamborg, S. Villaume, and J. N. Thépaut. The ERA5 global reanalysis. *Quarterly Journal of the Royal Meteorological Society*, 146(730):1999–2049, 2020. ISSN 1477870X. doi: 10.1002/qj.3803.

J. R. Jambeck, R. Geyer, C. Wilcox, T. R. Siegler, M. Perryman, A. Andrady, R. Narayan, and K. L. Law. Plastic waste inputs from land into the ocean. *Science*, 347 (6223):768–771, 2015. ISSN 00368075, 10959203. URL http://www.jstor.org/stable/24746131.

K. L. Law. Plastics in the Marine Environment. *Annual Review of Marine Science*, 9(1): 205–229, 2017. ISSN 19410611. doi: 10.1146/annurev-marine-010816-060409.

K. L. Law, S. E. Morét-Ferguson, D. S. Goodwin, E. R. Zettler, E. Deforce, T. Kukulka, and G. Proskurowski. Distribution of surface plastic debris in the eastern pacific ocean from an 11-year data set. *Environmental Science and Technology*, 48(9): 4732–4738, 5 2014. ISSN 15205851. doi: 10.1021/es4053076.

L. C. Lebreton, S. D. Greer, and J. C. Borrero. Numerical modelling of floating debris in the world's oceans. *Marine Pollution Bulletin*, 64(3):653–661, 2012. ISSN 0025326X. doi: 10.1016/j.marpolbul.2011.10.027. URL http://dx.doi.org/10.1016/j.marpolbul.2011.10.027.

L. C. Lebreton, J. Van Der Zwet, J. W. Damsteeg, B. Slat, A. Andrady, and J. Reisser. River plastic emissions to the world's oceans. *Nature Communications*, 8, 6 2017. ISSN 20411723. doi: 10.1038/ncomms15611.

R. Lumpkin, N. Maximenko, and M. Pazos. Evaluating where and why drifters die. *Journal of Atmospheric and Oceanic Technology*, 29(2):300–308, 2012. doi: 10.1175/JTECH-D-11-00100.1. URL https://journals.ametsoc.org/view/journals/atot/29/2/jtech-d-11-00100_1.xml.

R. Lumpkin, T. Özgökmen, and L. Centurioni. Advances in the Application of Surface Drifters Annual Reviews in Marine Science. *Annual Review of Marine Science*, page 59–81, 2017. doi: 10.1146/annurev-marine-010816-060641. URL https://doi.org/10.1146/annurev-marine-010816-060641.

C. Maes, B. Blanke, and E. Martinez. Origin and fate of surface drift in the oceanic convergence zones of the eastern Pacific. *Geophysical Research Letters*, 43(7):3398–3405, 4 2016. ISSN 19448007. doi: 10.1002/2016GL068217.

E. Martinez, K. Maamaatuaiahutapu, and V. Taillandier. Floating marine debris sur-

face drift: Convergence and accumulation toward the South Pacific subtropical gyre. *Marine Pollution Bulletin*, 58(9):1347–1355, 9 2009. ISSN 0025326X. doi: 10.1016/J.MARPOLBUL.2009.04.022.

N. Maximenko, J. Hafner, and P. Niiler. Pathways of marine debris derived from trajectories of Lagrangian drifters. *Marine Pollution Bulletin*, 65(1-3):51–62, 1 2012. ISSN 0025326X. doi: 10.1016/j.marpolbul.2011.04.016.

M. Menna, P.-M. Poulain, A. Bussani, and R. Gerin. Detecting the drogue presence of svp drifters from wind slippage in the mediterranean sea. *Measurement*, 125:447–453, 2018. ISSN 0263-2241. doi: 10.1016/j.measurement.2018.05.022. URL https://www.sciencedirect.com/science/article/pii/S0263224118304081.

P. Niiler. Chapter 4.1 the world ocean surface circulation. In G. Siedler, J. Church, and J. Gould, editors, *Ocean Circulation and Climate*, volume 77 of *International Geophysics*, page 193–204. Academic Press, 2001. doi: 10.1016/S0074-6142(01)80119-4. URL https://www.sciencedirect.com/science/article/pii/S0074614201801194.

P. P. Niiler, A. S. Sybrandy, K. Bi, P. M. Poulain, and D. Bitterman. Measurements of the water-following capability of holey-sock and TRISTAR drifters. *Deep Sea Research Part I: Oceanographic Research Papers*, 42(11-12):1951–1964, 11 1995. ISSN 0967-0637. doi: 10.1016/0967-0637(95)00076-3.

V. Onink, D. Wichmann, P. Delandmeter, and E. van Sebille. The Role of Ekman Currents, Geostrophy, and Stokes Drift in the Accumulation of Floating Microplastic. *Journal of Geophysical Research: Oceans*, 124(3):1474–1490, 3 2019. ISSN 21699291. doi: 10.1029/2018JC014547.

P. M. Poulain, R. Gerin, E. Mauri, and R. Pennel. Wind effects on drogued and undrogued drifters in the eastern Mediterranean. *Journal of Atmospheric and Oceanic Technology*, 26(6):1144–1156, 2009. ISSN 07390572. doi: 10.1175/2008JTECHO618.1.

N. A. Rayner, D. E. Parker, E. B. Horton, C. K. Folland, L. V. Alexander, D. P. Rowell, E. C. Kent, and A. Kaplan. Global analyses of sea surface temperature, sea ice, and night marine air temperature since the late nineteenth century. *J. Geophys. Res*, 108 (D14):4407, 2003. doi: 10.1029/2002JD002670. URL http://www.nsidc.org.

D. Roemmich and P. Sutton. The mean and variability of ocean circulation past northern new zealand: Determining the representativeness of hydrographic climatologies. *Journal of Geophysical Research: Oceans*, 103(C6):13041–13054, 1998. doi: https://doi.org/10.1029/98JC00583. URL https://agupubs.onlinelibrary.wiley.com/doi/abs/10.1029/98JC00583.

L. Stramma, R. G. Peterson, and M. Tomczak. The South Pacific Current. *Journal of Physical Oceanography*, 25(1):77–91, 1995. ISSN 00223670. doi: 10.1175/1520-0485(1995)025<0077:TSPC>2.0.CO;2.

G. Sutherland, N. Soontiens, F. Davidson, G. C. Smith, N. Bernier, H. Blanken, D. Schillinger, G. Marcotte, J. Röhrs, K. F. Dagestad, K. H. Christensen, and Ø. Breivik. Evaluating the leeway coefficient of ocean drifters using operational marine environmental prediction systems. *Journal of Atmospheric and Oceanic Technology*, 37(11):1943–1954, 2020. ISSN 15200426. doi: 10.1175/JTECH-D-20-0013.1.

L. D. Talley, G. L. Pickard, W. J. Emery, and J. H. Swift. Pacific Ocean. *Descriptive Physical Oceanography*, page 303–362, 1 2011. doi: 10.1016/B978-0-7506-4552-2.10010-1.

G. K. Vallis. *Atmospheric and Oceanic Fluid Dynamics*. Cambridge University Press, 6 2017. ISBN 9781107065505. doi: 10.1017/9781107588417. URL https://www.cambridge.org/core/product/identifier/9781107588417/type/book.

E. Van Sebille, M. H. England, and G. Froyland. Origin, dynamics and evolution of ocean garbage patches from observed surface drifters. *Environmental Research Letters*, 7(4), 2012. ISSN 17489326. doi: 10.1088/1748-9326/7/4/044040.

E. Van Sebille, C. Wilcox, L. Lebreton, N. Maximenko, B. D. Hardesty, J. A. Van Franeker, M. Eriksen, D. Siegel, F. Galgani, and K. L. Law. A global inventory of small floating plastic debris. *Environmental Research Letters*, 10(12), 2015. ISSN 17489326. doi: 10.1088/1748-9326/10/12/124006.

E. van Sebille, S. M. Griffies, R. Abernathey, T. P. Adams, P. Berloff, A. Biastoch, B. Blanke, E. P. Chassignet, Y. Cheng, C. J. Cotter, E. Deleersnijder, K. Döös, H. F. Drake, S. Drijfhout, S. F. Gary, A. W. Heemink, J. Kjellsson, I. M. Koszalka, M. Lange, C. Lique, G. A. MacGilchrist, R. Marsh, C. G. Mayorga Adame, R. McAdam, F. Nencioli, C. B. Paris, M. D. Piggott, J. A. Polton, S. Rühs, S. H. Shah, M. D. Thomas, J. Wang, P. J. Wolfram, L. Zanna, and J. D. Zika. Lagrangian ocean analysis: Fundamentals and practices. *Ocean Modelling*, 121(October 2017):49–75, 2018. ISSN 14635003. doi: 10.1016/j.ocemod.2017.11.008.

M. R. M. Zaki and A. Z. Aris. An overview of the effects of nanoplastics on marine organisms. *Science of The Total Environment*, 831:154757, 7 2022. ISSN 0048-9697. doi: 10.1016/J.SCITOTENV.2022.154757.

H. Zuo, M. A. Balmaseda, S. Tietsche, K. Mogensen, and M. Mayer. The ECMWF operational ensemble reanalysis–analysis system for ocean and sea ice: a description of the system and assessment. *Ocean Science*, 15(3):779–808, 6 2019. ISSN 1812-0792. doi: 10.5194/os-15-779-2019. URL https://os.copernicus.org/articles/15/779/2019/.

A Drifters

A.1 Drogued Drifters

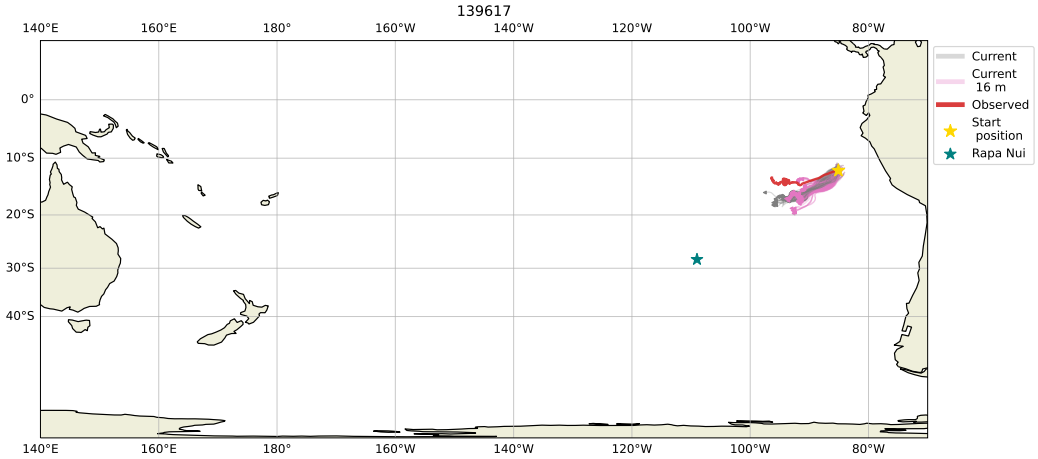

Figure 19: The observed trajectory of the drogued drifter 139617 (red), the virtual drifters forced with only the surface currents (grey), and the virtual drifters forced with currents from a depth of 16 meters (pink). The triangles mark the end positions of the virtual particles. The yellow star indicates the drifter's deployment position and the virtual drifters' seeding point. The teal star marks the position of the island Rapa Nui.

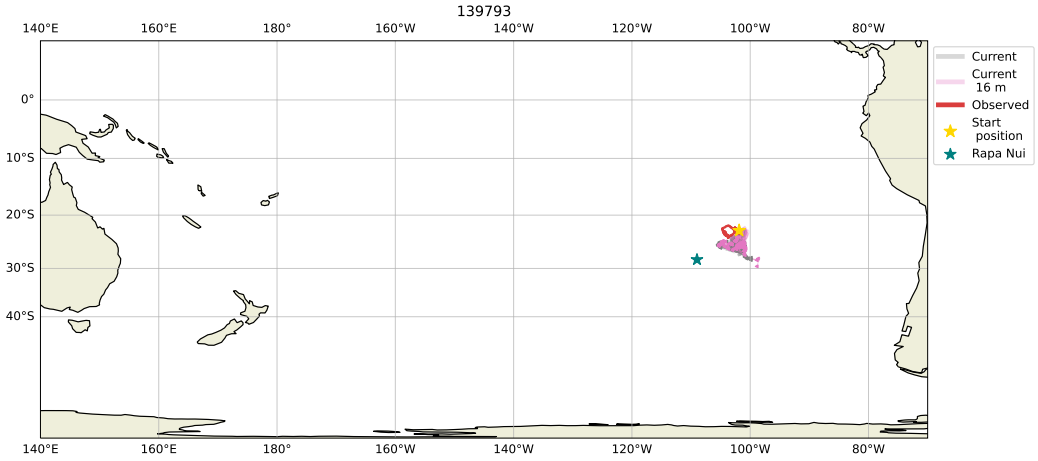

Figure 20: The observed trajectory of the drogued drifter 139793 (red), the virtual drifters forced with only the surface currents (grey), and the virtual drifters forced with currents from a depth of 16 meters (pink). The triangles mark the end positions of the virtual particles. The yellow star indicates the drifter's deployment position and the virtual drifters' seeding point. The teal star marks the position of the island Rapa Nui.

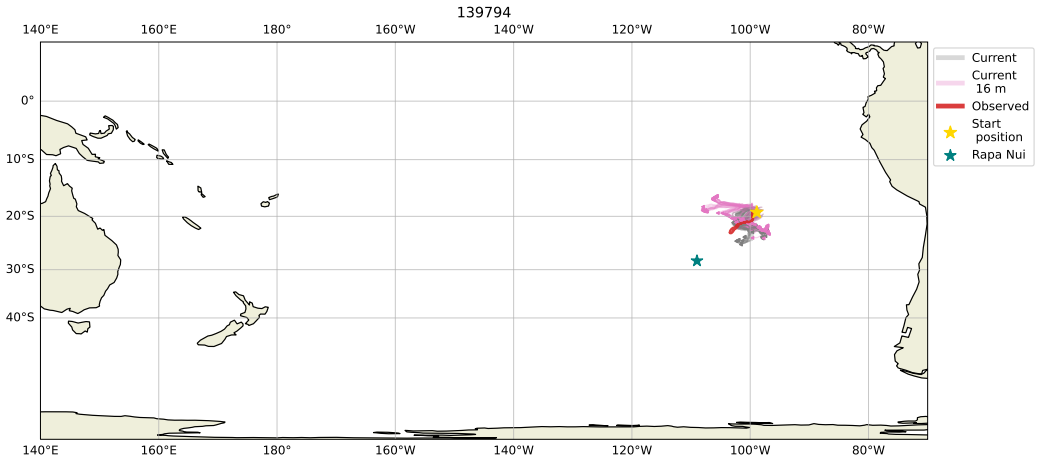

Figure 21: The observed trajectory of the drogued drifter 139794 (red), the virtual drifters forced with only the surface currents (grey), and the virtual drifters forced with currents from a depth of 16 meters (pink). The triangles mark the end positions of the virtual particles. The yellow star indicates the drifter's deployment position and the virtual drifters' seeding point. The teal star marks the position of the island Rapa Nui.

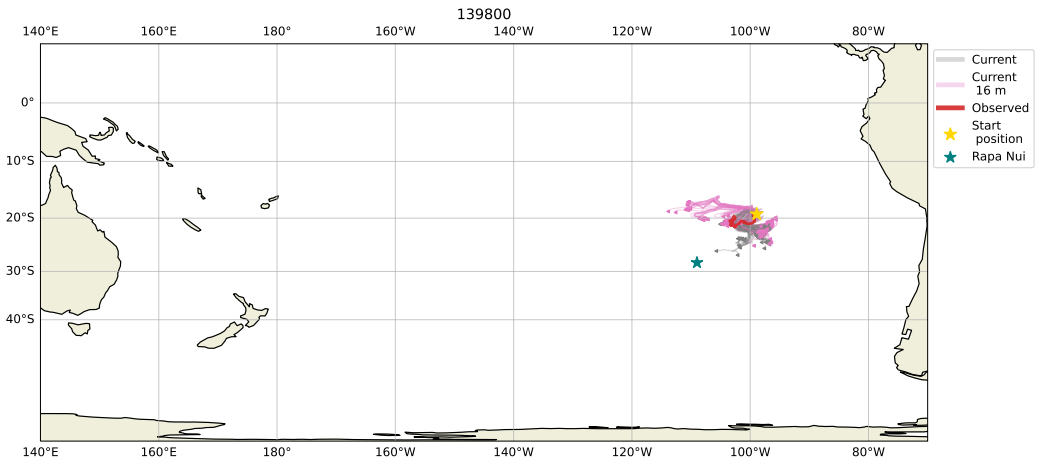

Figure 25: The observed trajectory of the drogued drifter 139800 (red), the virtual drifters forced with only the surface currents (grey), and the virtual drifters forced with currents from a depth of 16 meters (pink). The triangles mark the end positions of the virtual particles. The yellow star indicates the drifter's deployment position and the virtual drifters' seeding point. The teal star marks the position of the island Rapa Nui.

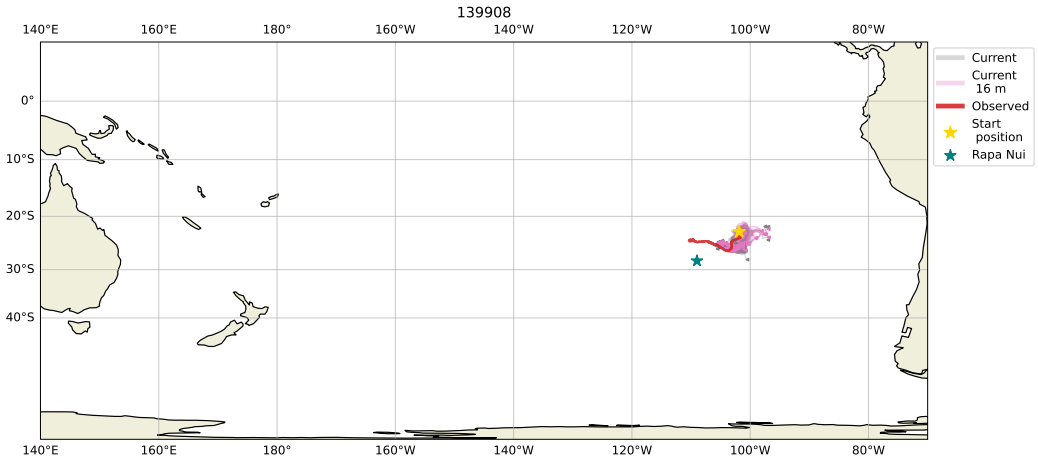

Figure 26: The observed trajectory of the drogued drifter 139908 (red), the virtual drifters forced with only the surface currents (grey), and the virtual drifters forced with currents from a depth of 16 meters (pink). The triangles mark the end positions of the virtual particles. The yellow star indicates the drifter's deployment position and the virtual drifters' seeding point. The teal star marks the position of the island Rapa Nui.

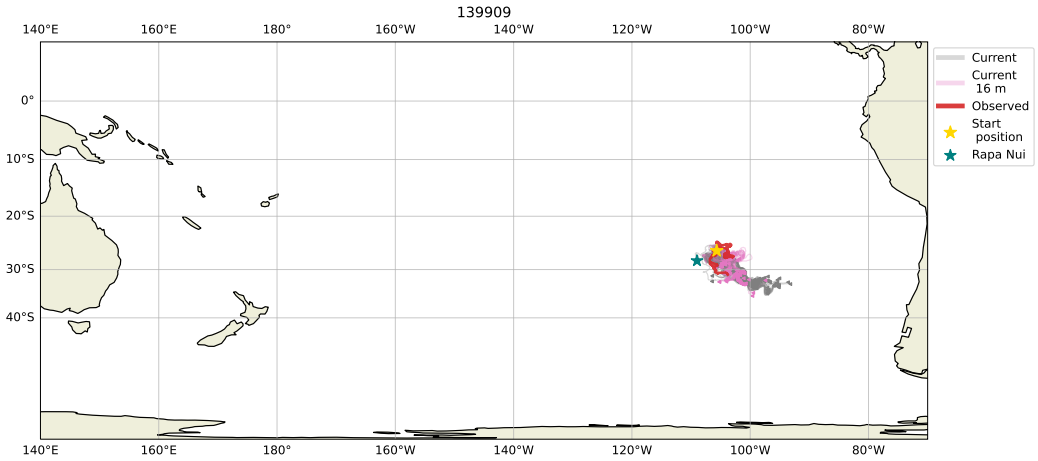

Figure 27: The observed trajectory of the drogued drifter 139908 (red), the virtual drifters forced with only the surface currents (grey), and the virtual drifters forced with currents from a depth of 16 meters (pink). The triangles mark the end positions of the virtual particles. The yellow star indicates the drifter's deployment position and the virtual drifters' seeding point. The teal star marks the position of the island Rapa Nui.

A.2 Undrogued Drifters

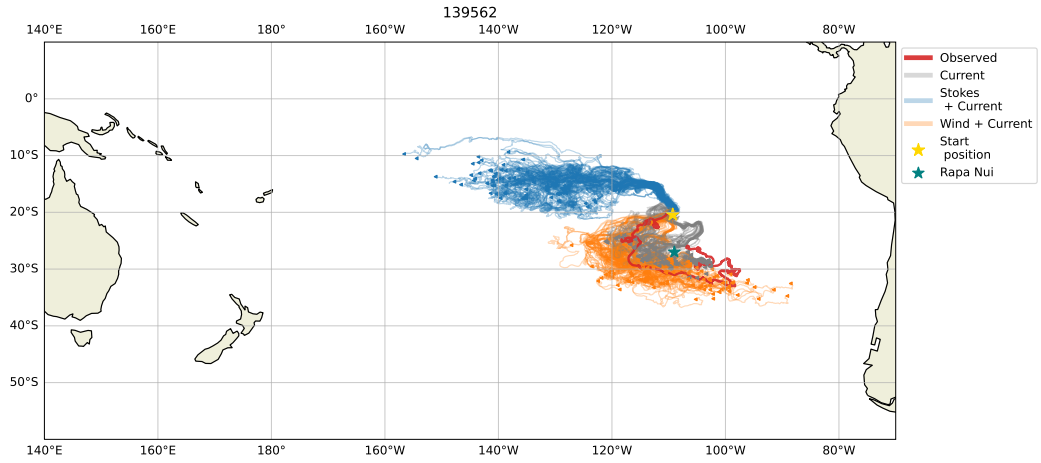

Figure 28: The observed trajectory (red) for the undrogued drifter 139562, the virtual drifters forced with only the surface currents (grey), the virtual drifters forced with a combination of Stokes drift and surface currents (blue) and the virtual drifters forced with surface currents and wind. The triangles mark the end positions of the virtual particles. The yellow star indicates the drifter's deployment position and the virtual drifters' seeding point. The teal star marks the position of the island Rapa Nui.

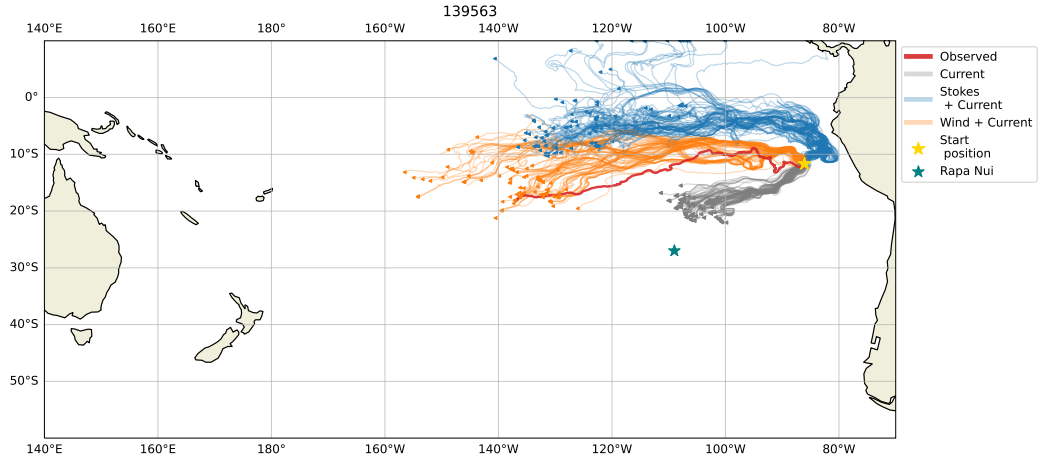

Figure 29: The observed trajectory (red) for the undrogued drifter 139563, the virtual drifters forced with only the surface currents (grey), the virtual drifters forced with a combination of Stokes drift and surface currents (blue) and the virtual drifters forced with surface currents and wind. The triangles mark the end positions of the virtual particles. The yellow star indicates the drifter's deployment position and the virtual drifters' seeding point. The teal star marks the position of the island Rapa Nui.

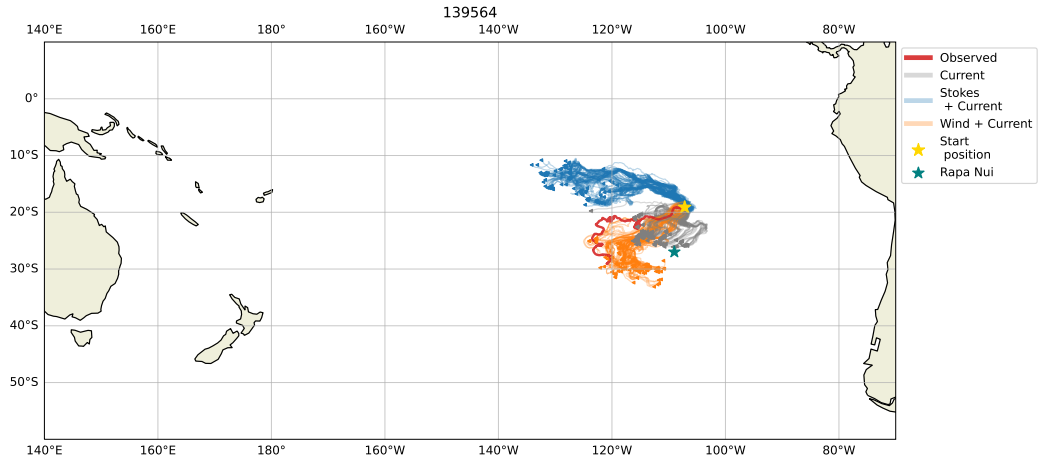

Figure 30: The observed trajectory (red) for the undrogued drifter 139564, the virtual drifters forced with only the surface currents (grey), the virtual drifters forced with a combination of Stokes drift and surface currents (blue) and the virtual drifters forced with surface currents and wind. The triangles mark the end positions of the virtual particles. The yellow star indicates the drifter's deployment position and the virtual drifters' seeding point. The teal star marks the position of the island Rapa Nui.

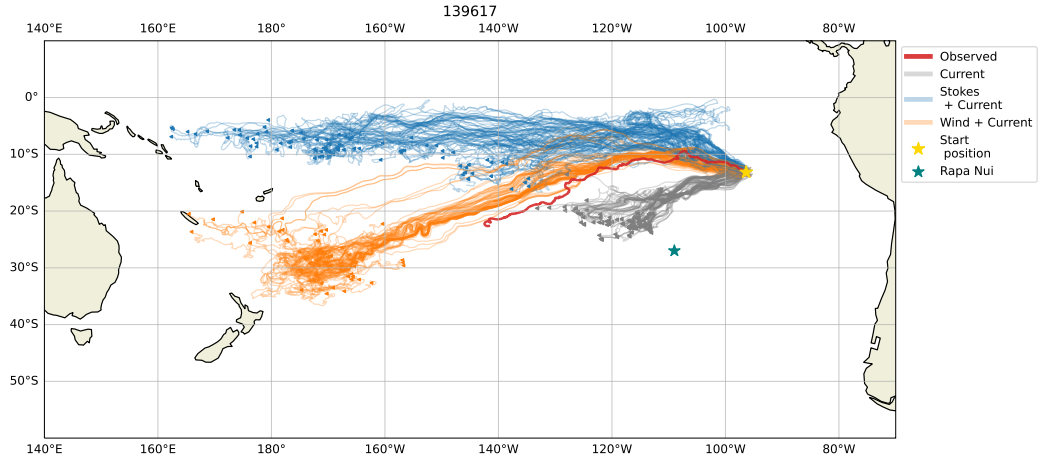

Figure 31: The observed trajectory (red) for the undrogued drifter 1395617, the virtual drifters forced with only the surface currents (grey), the virtual drifters forced with a combination of Stokes drift and surface currents (blue) and the virtual drifters forced with surface currents and wind. The triangles mark the end positions of the virtual particles. The yellow star indicates the drifter's deployment position and the virtual drifters' seeding point. The teal star marks the position of the island Rapa Nui.

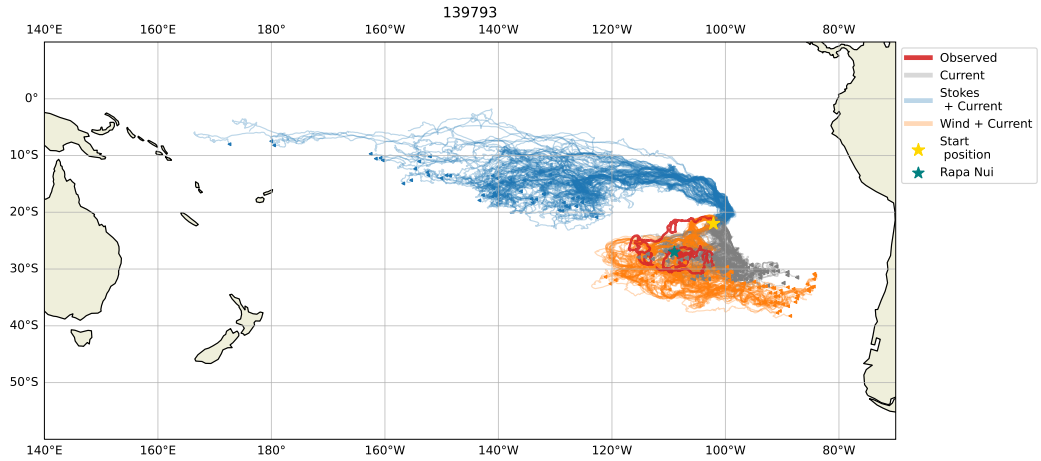

Figure 32: The observed trajectory (red) for the undrogued drifter 139793, the virtual drifters forced with only the surface currents (grey), the virtual drifters forced with a combination of Stokes drift and surface currents (blue) and the virtual drifters forced with surface currents and wind. The triangles mark the end positions of the virtual particles. The yellow star indicates the drifter's deployment position and the virtual drifters' seeding point. The teal star marks the position of the island Rapa Nui.

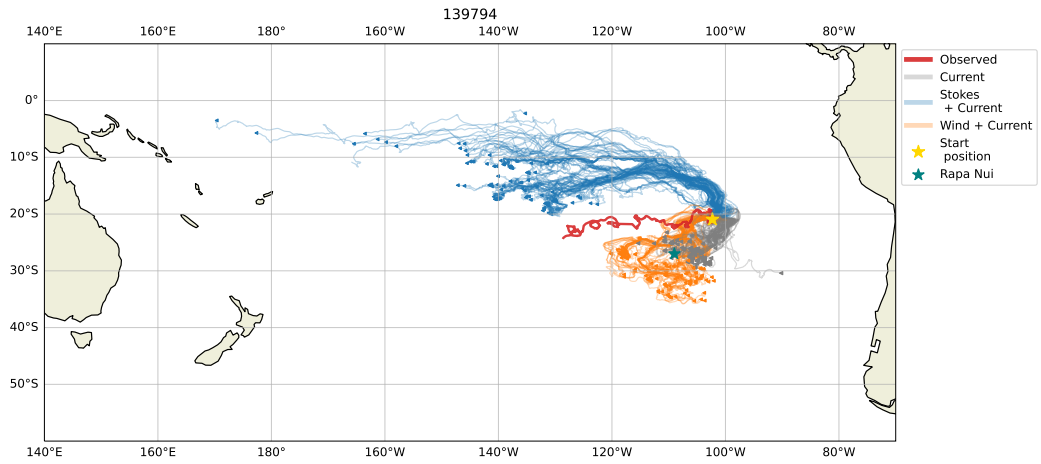

Figure 33: The observed trajectory (red) for the undrogued drifter 139794, the virtual drifters forced with only the surface currents (grey), the virtual drifters forced with a combination of Stokes drift and surface currents (blue) and the virtual drifters forced with surface currents and wind. The triangles mark the end positions of the virtual particles. The yellow star indicates the drifter's deployment position and the virtual drifters' seeding point. The teal star marks the position of the island Rapa Nui.

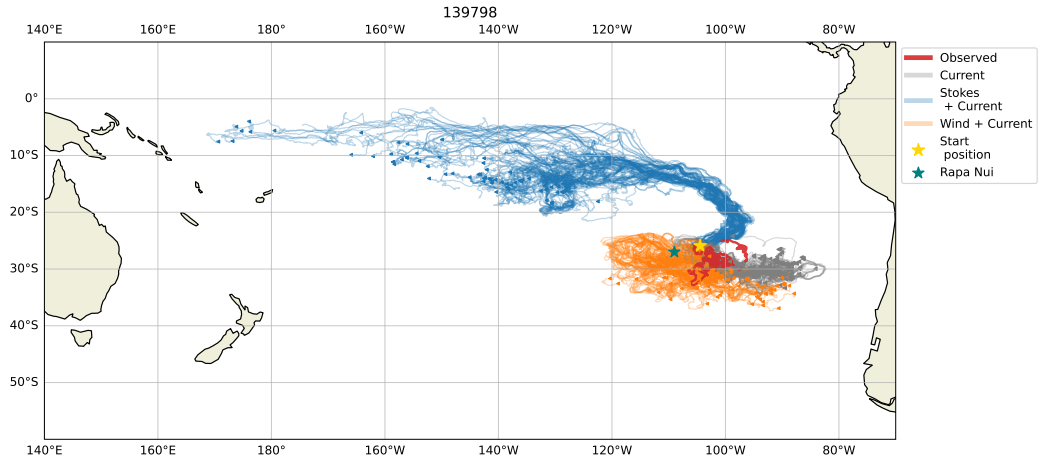

Figure 34: The observed trajectory (red) for the undrogued drifter 139798, the virtual drifters forced with only the surface currents (grey), the virtual drifters forced with a combination of Stokes drift and surface currents (blue) and the virtual drifters forced with surface currents and wind. The triangles mark the end positions of the virtual particles. The yellow star indicates the drifter's deployment position and the virtual drifters' seeding point. The teal star marks the position of the island Rapa Nui.

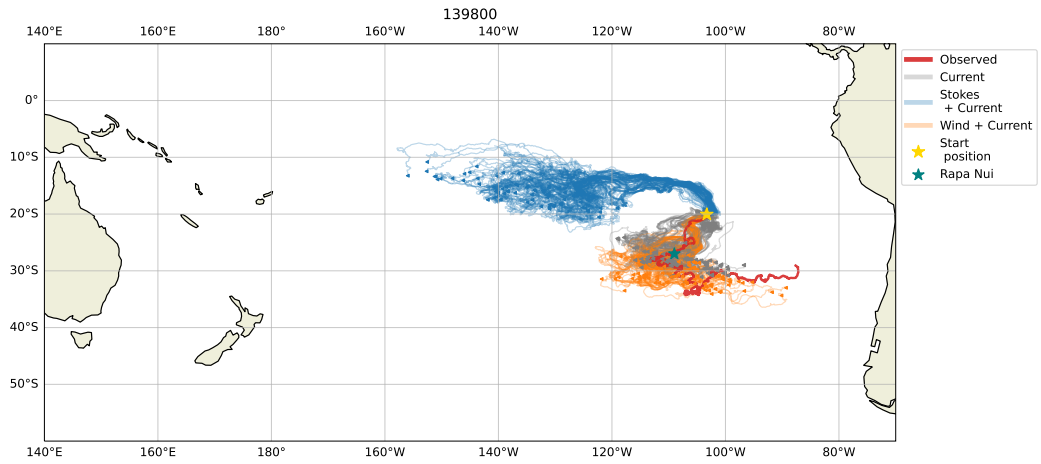

Figure 35: The observed trajectory (red) for the undrogued drifter 139800, the virtual drifters forced with only the surface currents (grey), the virtual drifters forced with a combination of Stokes drift and surface currents (blue) and the virtual drifters forced with surface currents and wind. The triangles mark the end positions of the virtual particles. The yellow star indicates the drifter's deployment position and the virtual drifters' seeding point. The teal star marks the position of the island Rapa Nui.

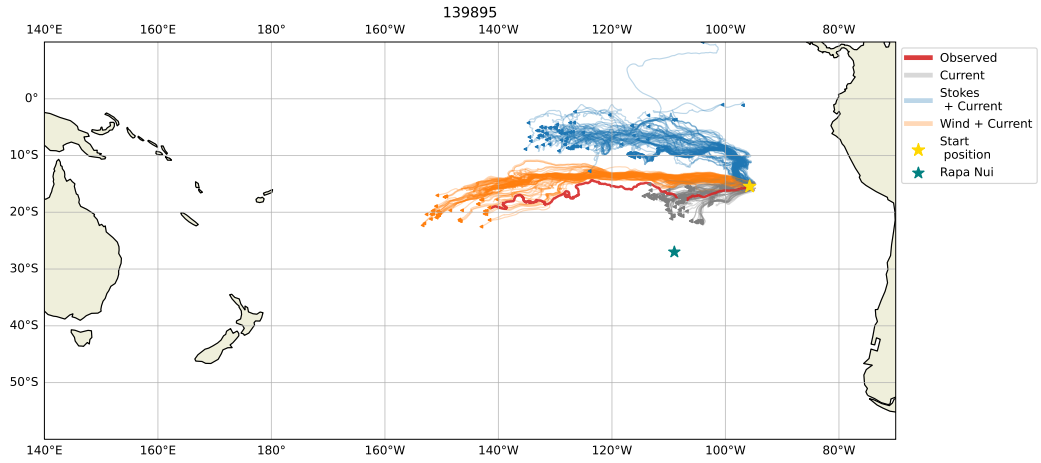

Figure 36: The observed trajectory (red) for the undrogued drifter 139895, the virtual drifters forced with only the surface currents (grey), the virtual drifters forced with a combination of Stokes drift and surface currents (blue) and the virtual drifters forced with surface currents and wind. The triangles mark the end positions of the virtual particles. The yellow star indicates the drifter's deployment position and the virtual drifters' seeding point. The teal star marks the position of the island Rapa Nui.

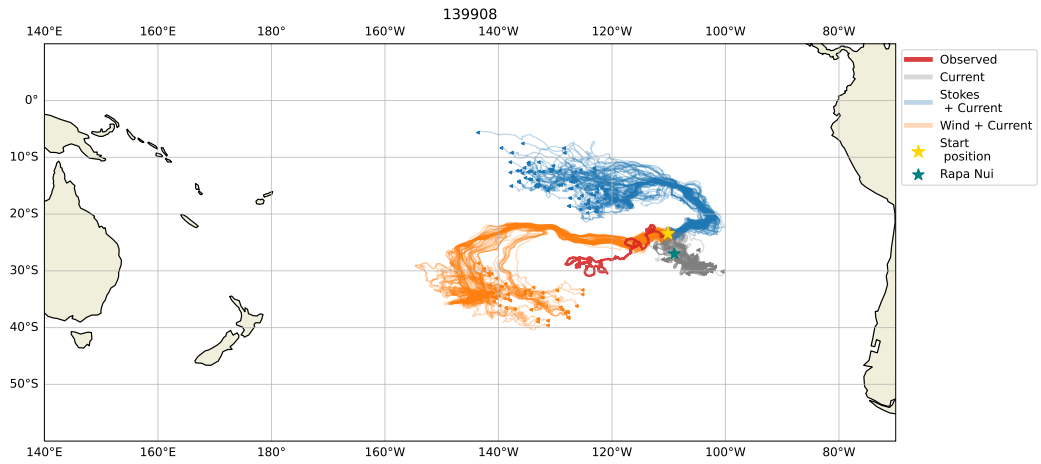

Figure 37: The observed trajectory (red) for the undrogued drifter 139908, the virtual drifters forced with only the surface currents (grey), the virtual drifters forced with a combination of Stokes drift and surface currents (blue) and the virtual drifters forced with surface currents and wind. The triangles mark the end positions of the virtual particles. The yellow star indicates the drifter's deployment position and the virtual drifters' seeding point. The teal star marks the position of the island Rapa Nui.

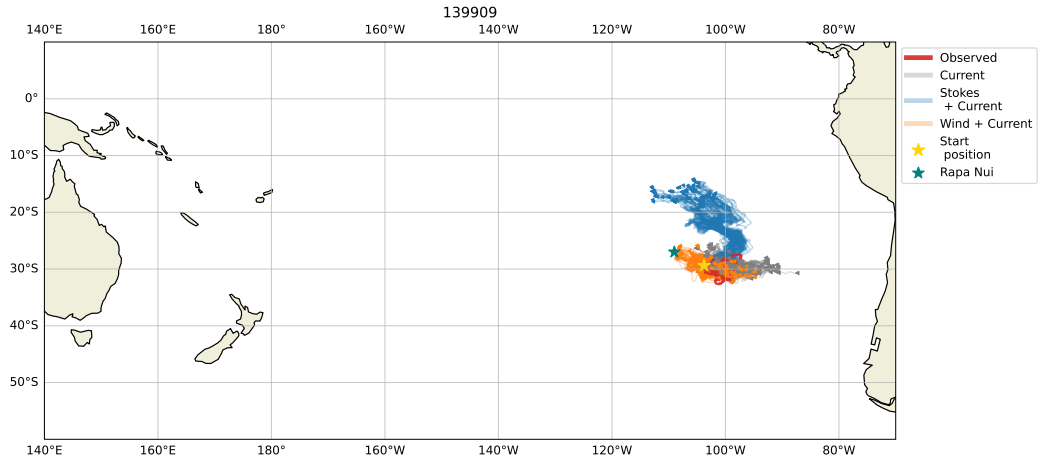

Figure 38: The observed trajectory (red) for the undrogued drifter 139909, the virtual drifters forced with only the surface currents (grey), the virtual drifters forced with a combination of Stokes drift and surface currents (blue) and the virtual drifters forced with surface currents and wind. The triangles mark the end positions of the virtual particles. The yellow star indicates the drifter's deployment position and the virtual drifters' seeding point. The teal star marks the position of the island Rapa Nui.

A.3 Leeway Coefficient

A.3.1 Drogued

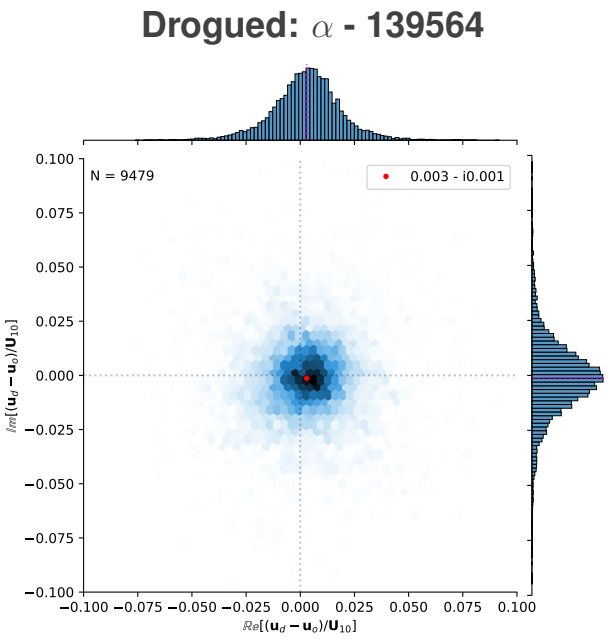

Figure 39: 2D histogram of the leeway coefficient, $\boldsymbol{\alpha}$ (implicit Stokes drift), and the corresponding 1D histograms for the along-wind and cross-wind components for the drogued drifter 139564, with the drogue, forced with the currents at 16 meters depth from ORAS5 and winds from ERA5. The red dot and lines indicate the mean. Figure provided by Graig Sutherland

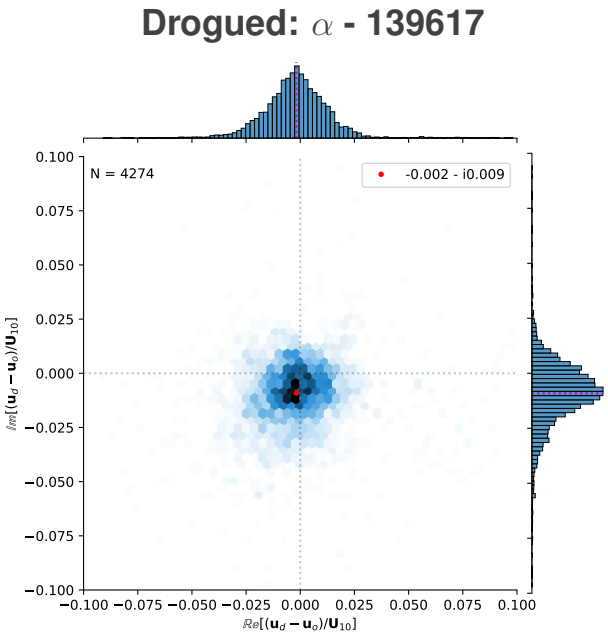

Figure 40: 2D histogram of the leeway coefficient, $\boldsymbol{\alpha}$ (implicit Stokes drift), and the corresponding 1D histograms for the along-wind and cross-wind components for the drogued drifter 139617, with the drogue, forced with the currents at 16 meters depth from ORAS5 and winds from ERA5. The red dot and lines indicate the mean. Figure provided by Graig Sutherland

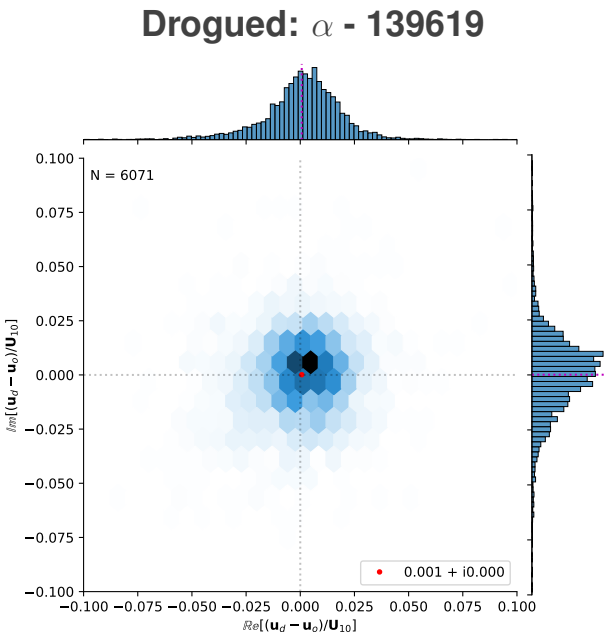

Figure 41: 2D histogram of the leeway coefficient, $\boldsymbol{\alpha}$ (implicit Stokes drift), and the corresponding 1D histograms for the along-wind and cross-wind components for the drogued drifter 139619, with the drogue, forced with the currents at 16 meters depth from ORAS5 and winds from ERA5. The red dot and lines indicate the mean. Figure provided by Graig Sutherland

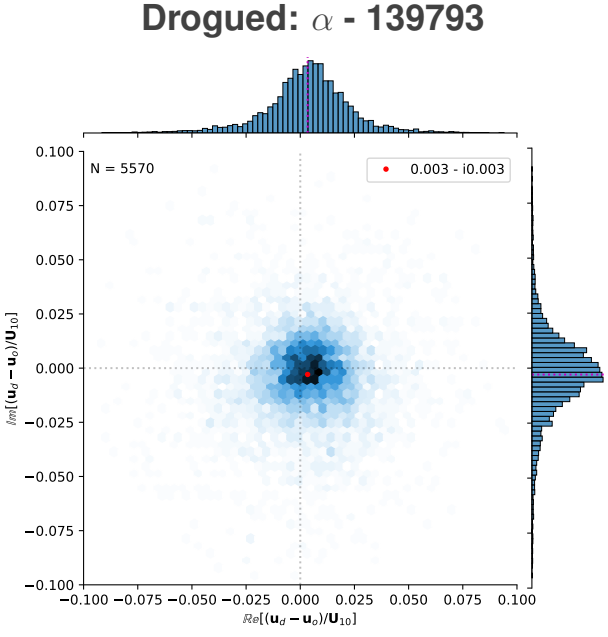

Figure 42: 2D histogram of the leeway coefficient, $\boldsymbol{\alpha}$ (implicit Stokes drift), and the corresponding 1D histograms for the along-wind and cross-wind components for the drogued drifter 139793, with the drogue, forced with the currents at 16 meters depth from ORAS5 and winds from ERA5. The red dot and lines indicate the mean. Figure provided by Graig Sutherland

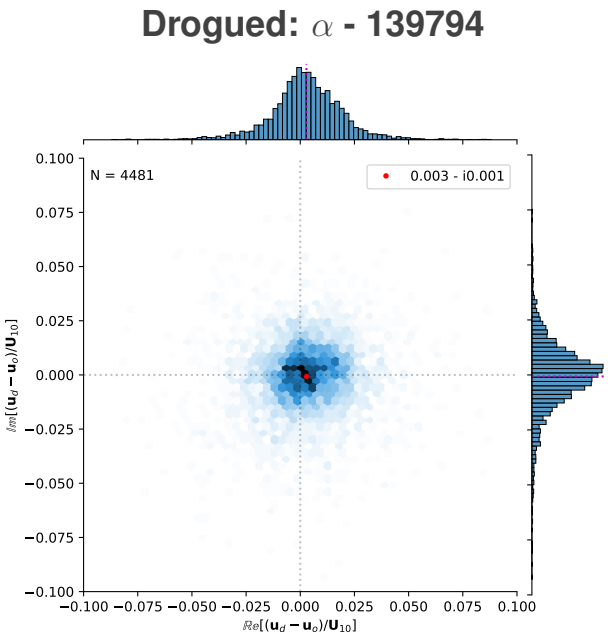

Figure 43: 2D histogram of the leeway coefficient, $\boldsymbol{\alpha}$ (implicit Stokes drift), and the corresponding 1D histograms for the along-wind and cross-wind components for the drogued drifter 139794, with the drogue, forced with the currents at 16 meters depth from ORAS5 and winds from ERA5. The red dot and lines indicate the mean. Figure provided by Graig Sutherland

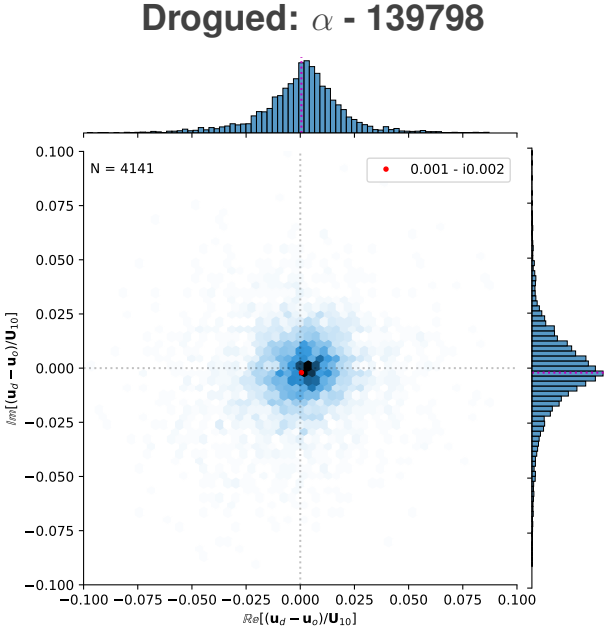

Figure 44: 2D histogram of the leeway coefficient, $\boldsymbol{\alpha}$ (implicit Stokes drift), and the corresponding 1D histograms for the along-wind and cross-wind components for the drogued drifter 139798, with the drogue, forced with the currents at 16 meters depth from ORAS5 and winds from ERA5. The red dot and lines indicate the mean. Figure provided by Graig Sutherland

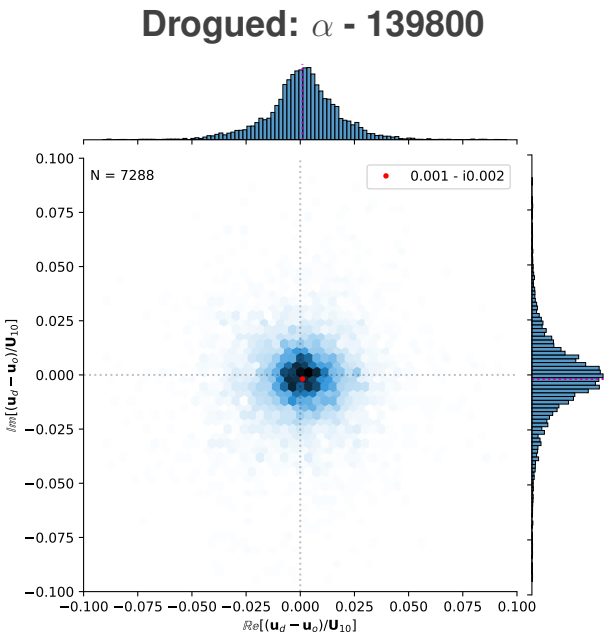

Figure 45: 2D histogram of the leeway coefficient, $\boldsymbol{\alpha}$ (implicit Stokes drift), and the corresponding 1D histograms for the along-wind and cross-wind components for the drogued drifter 139800, with the drogue, forced with the currents at 16 meters depth from ORAS5 and winds from ERA5. The red dot and lines indicate the mean. Figure provided by Graig Sutherland

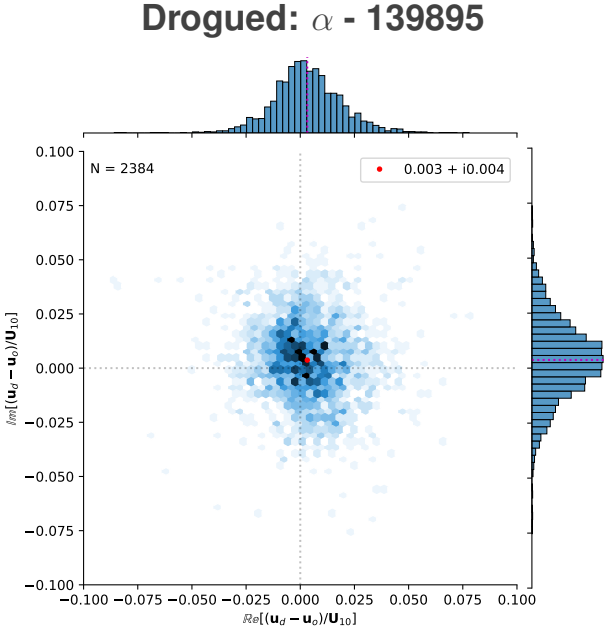

Figure 46: 2D histogram of the leeway coefficient, $\boldsymbol{\alpha}$ (implicit Stokes drift), and the corresponding 1D histograms for the along-wind and cross-wind components for the drogued drifter 139895, with the drogue, forced with the currents at 16 meters depth from ORAS5 and winds from ERA5. The red dot and lines indicate the mean. Figure provided by Graig Sutherland

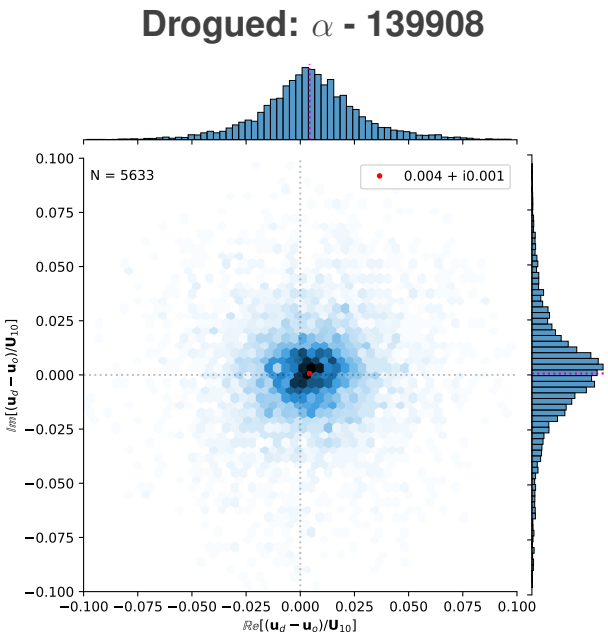

Figure 47: 2D histogram of the leeway coefficient, $\boldsymbol{\alpha}$ (implicit Stokes drift), and the corresponding 1D histograms for the along-wind and cross-wind components for the drogued drifter 139908, with the drogue, forced with the currents at 16 meters depth from ORAS5 and winds from ERA5. The red dot and lines indicate the mean. Figure provided by Graig Sutherland

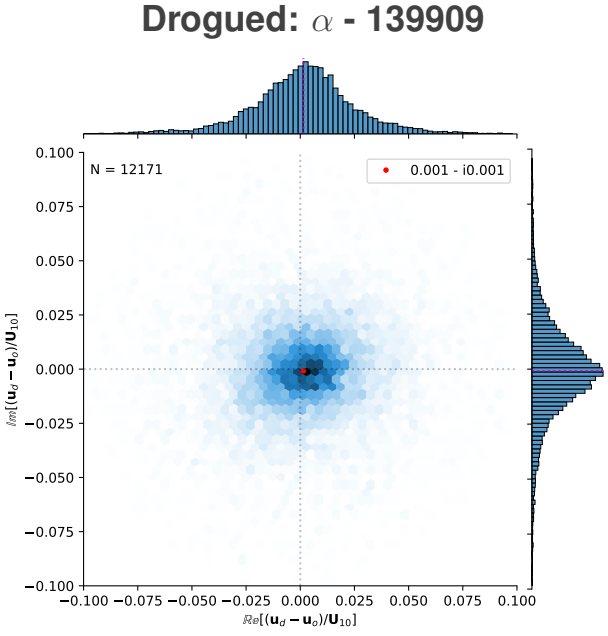

Figure 48: 2D histogram of the leeway coefficient, $\boldsymbol{\alpha}$ (implicit Stokes drift), and the corresponding 1D histograms for the along-wind and cross-wind components for the drogued drifter 139909, with the drogue, forced with the currents at 16 meters depth from ORAS5 and winds from ERA5. The red dot and lines indicate the mean. Figure provided by Graig Sutherland

A.3.2 Undrogued

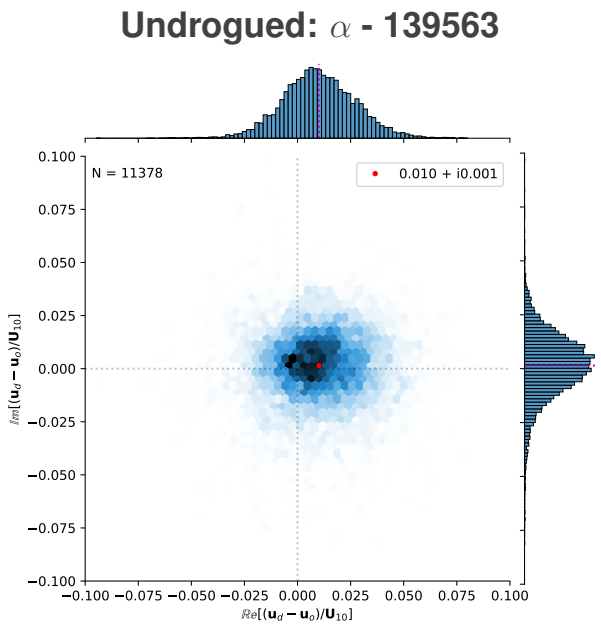

(a)

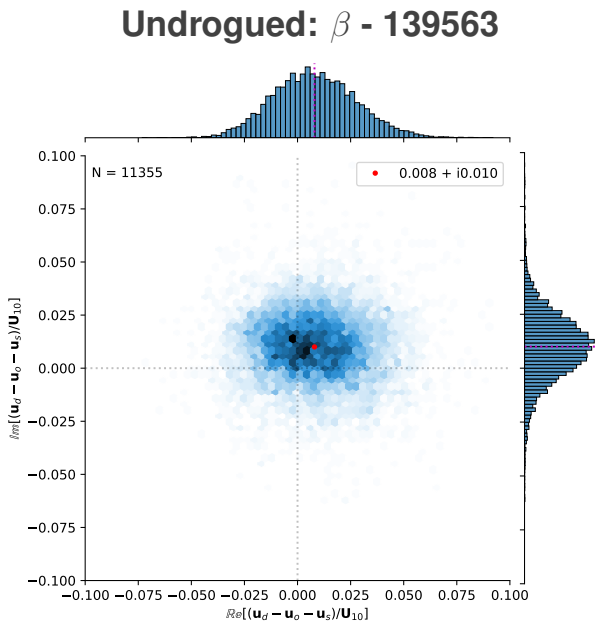

(b)

Figure 49: 2D histograms of the leeway coefficients and the corresponding histograms for the along-wind and cross-wind components for drifter 139563 after drogue is lost. (a) $\boldsymbol{\alpha}$ forced with surface currents from ORAS5 and winds from ERA5. (b) $\boldsymbol{\beta}$ with the Stokes drift explicitly included from ERA5. Figures provided by Graig Sutherland.

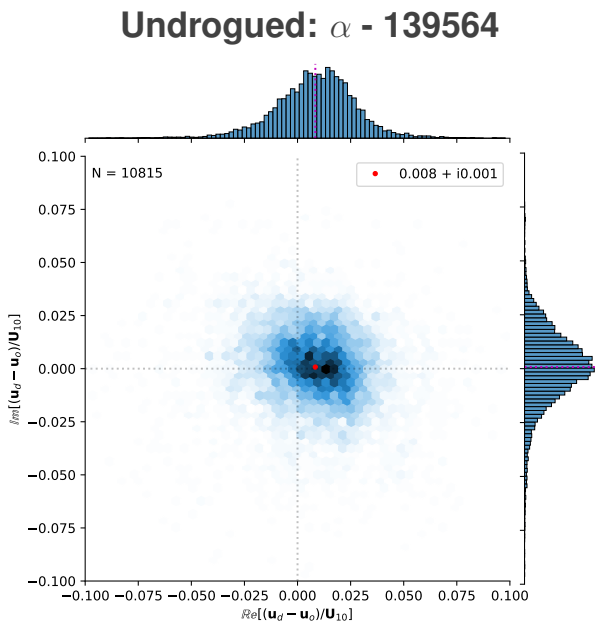

(a)

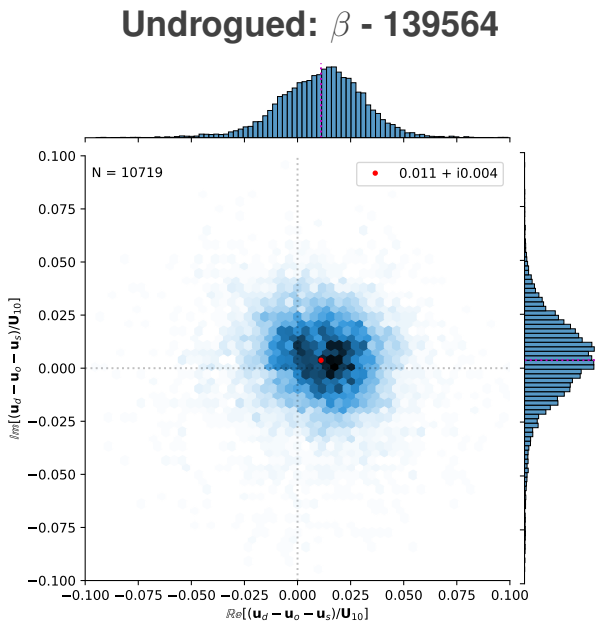

(b)

Figure 50: 2D histograms of the leeway coefficients and the corresponding histograms for the along-wind and cross-wind components for drifter 139564 after drogue is lost. (a) $\boldsymbol{\alpha}$ forced with surface currents from ORAS5 and winds from ERA5. (b) $\boldsymbol{\beta}$ with the Stokes drift explicitly included from ERA5. Figures provided by Graig Sutherland.

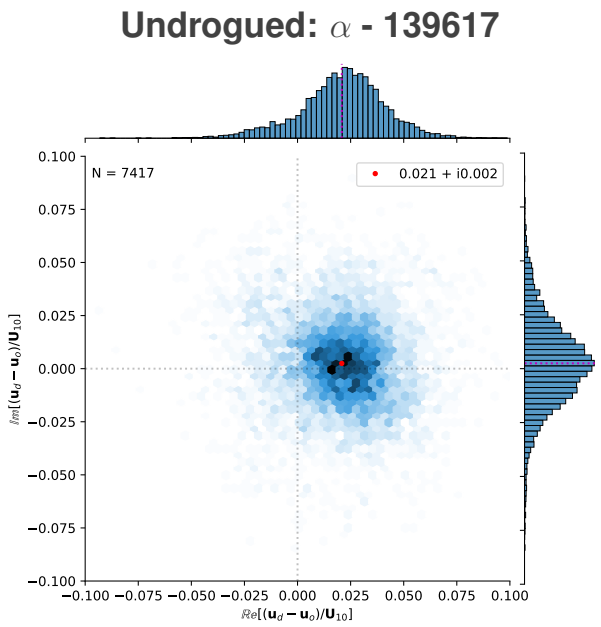

(a)

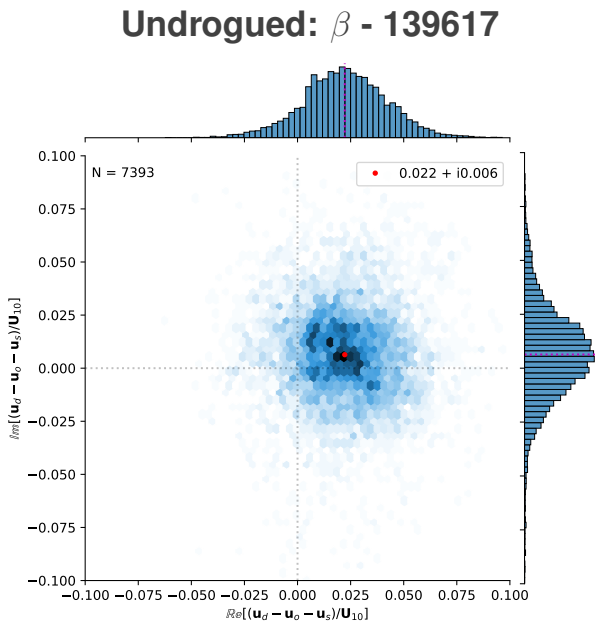

(b)

Figure 51: 2D histograms of the leeway coefficients and the corresponding histograms for the along-wind and cross-wind components for drifter 139617 after drogue is lost. (a) $\boldsymbol{\alpha}$ forced with surface currents from ORAS5 and winds from ERA5. (b) $\boldsymbol{\beta}$ with the Stokes drift explicitly included from ERA5. Figures provided by Graig Sutherland.

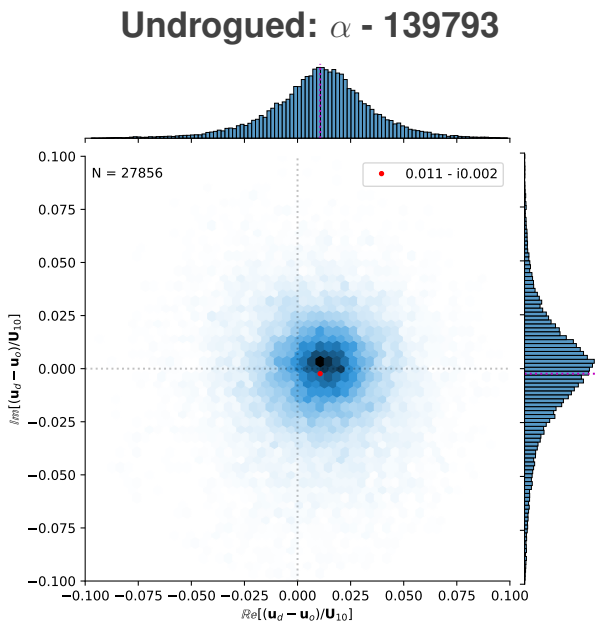

(a)

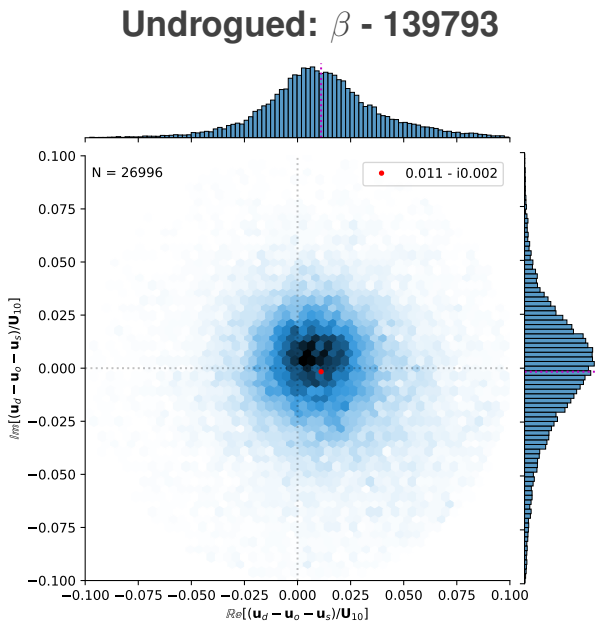

(b)

Figure 52: 2D histograms of the leeway coefficients and the corresponding histograms for the along-wind and cross-wind components for drifter 139793 after drogue is lost. (a) $\boldsymbol{\alpha}$ forced with surface currents from ORAS5 and winds from ERA5. (b) $\boldsymbol{\beta}$ with the Stokes drift explicitly included from ERA5. Figures provided by Graig Sutherland.

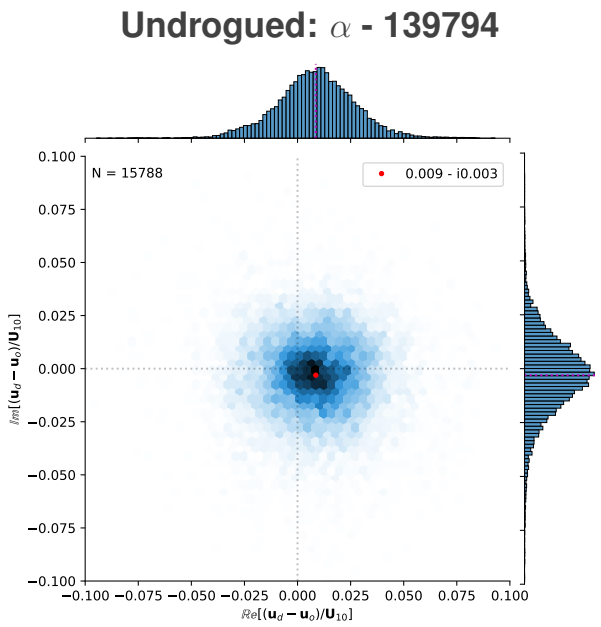

(a)

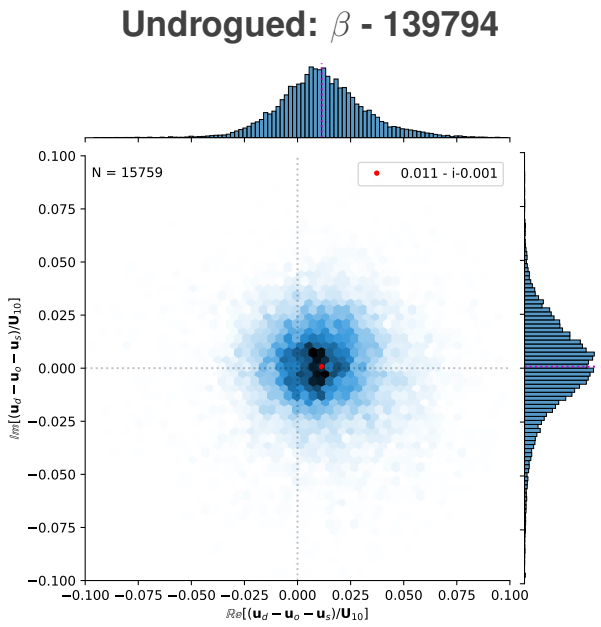

(b)

Figure 53: 2D histograms of the leeway coefficients and the corresponding histograms for the along-wind and cross-wind components for drifter 139794 after drogue is lost. (a) $\boldsymbol{\alpha}$ forced with surface currents from ORAS5 and winds from ERA5. (b) $\boldsymbol{\beta}$ with the Stokes drift explicitly included from ERA5. Figures provided by Graig Sutherland.

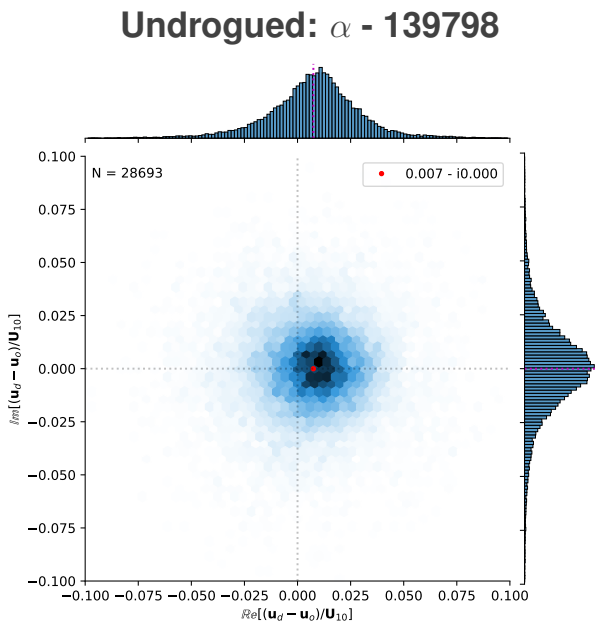

(a)

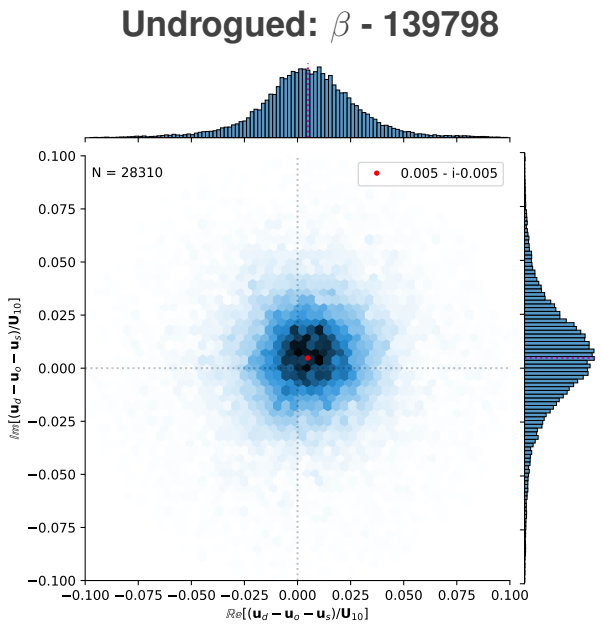

(b)

Figure 54: 2D histograms of the leeway coefficients and the corresponding histograms for the along-wind and cross-wind components for drifter 139798 after drogue is lost. (a) $\boldsymbol{\alpha}$ forced with surface currents from ORAS5 and winds from ERA5. (b) $\boldsymbol{\beta}$ with the Stokes drift explicitly included from ERA5. Figures provided by Graig Sutherland.

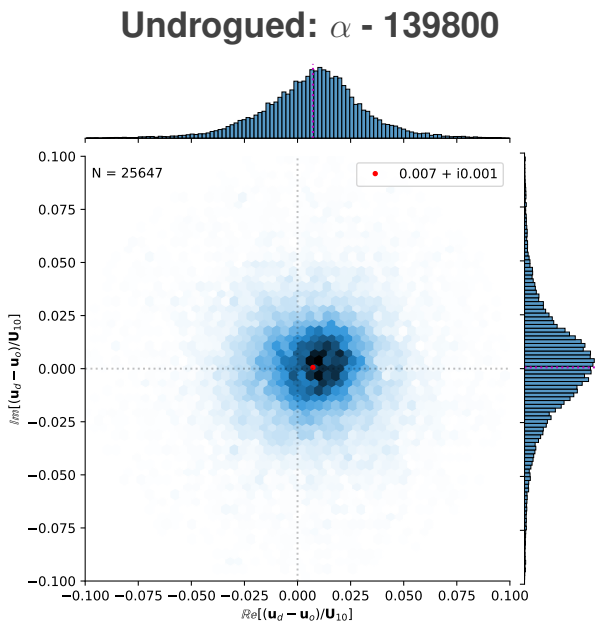

(a)

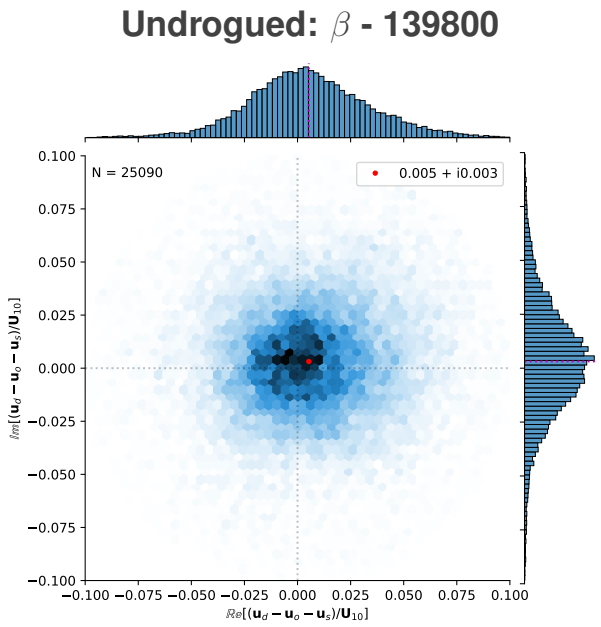

(b)

Figure 55: 2D histograms of the leeway coefficients and the corresponding histograms for the along-wind and cross-wind components for drifter 139800 after drogue is lost. (a) $\boldsymbol{\alpha}$ forced with surface currents from ORAS5 and winds from ERA5. (b) $\boldsymbol{\beta}$ with the Stokes drift explicitly included from ERA5. Figures provided by Graig Sutherland.

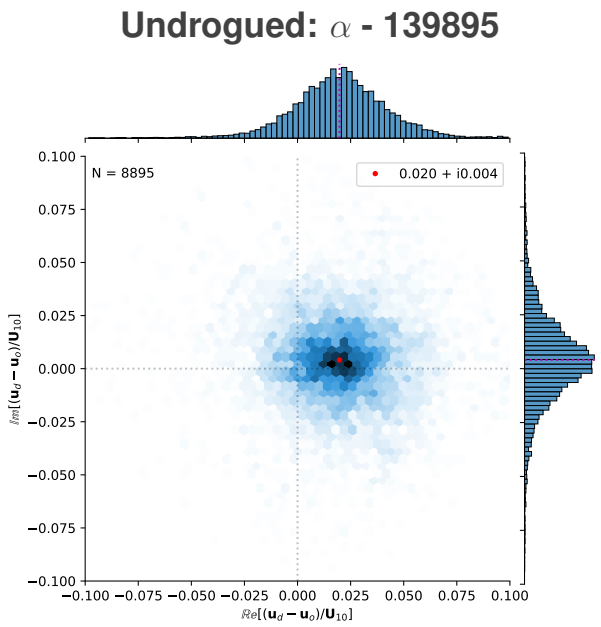

(a)

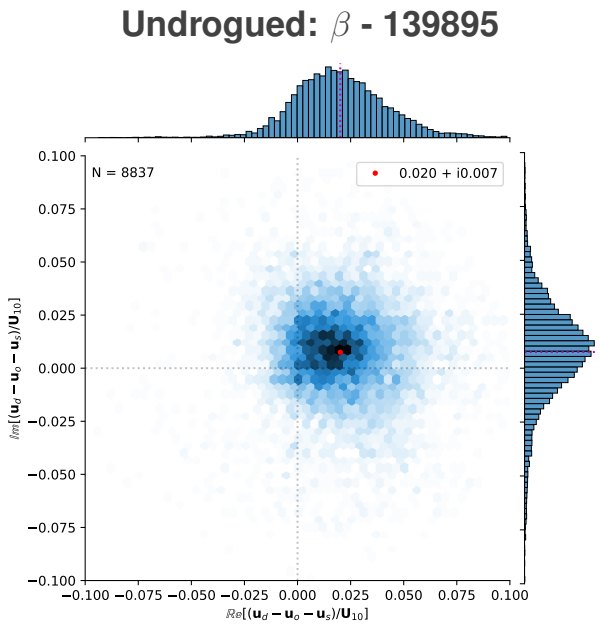

(b)

Figure 56: 2D histograms of the leeway coefficients and the corresponding histograms for the along-wind and cross-wind components for drifter 139895 after drogue is lost. (a) $\boldsymbol{\alpha}$ forced with surface currents from ORAS5 and winds from ERA5. (b) $\boldsymbol{\beta}$ with the Stokes drift explicitly included from ERA5. Figures provided by Graig Sutherland.

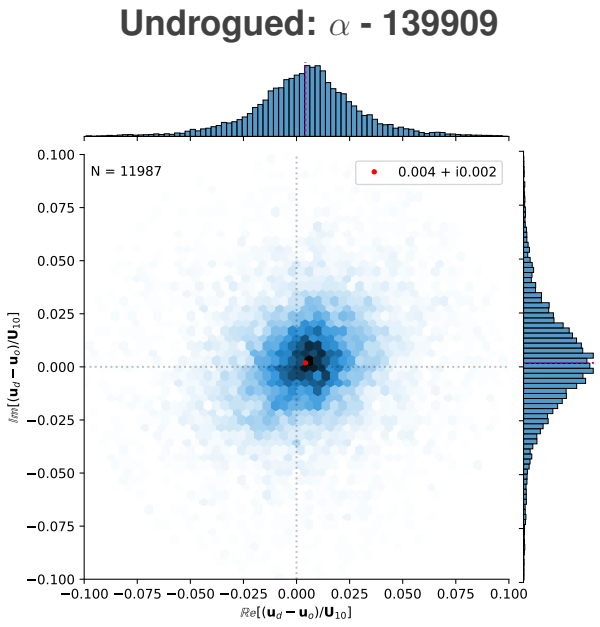

(a)

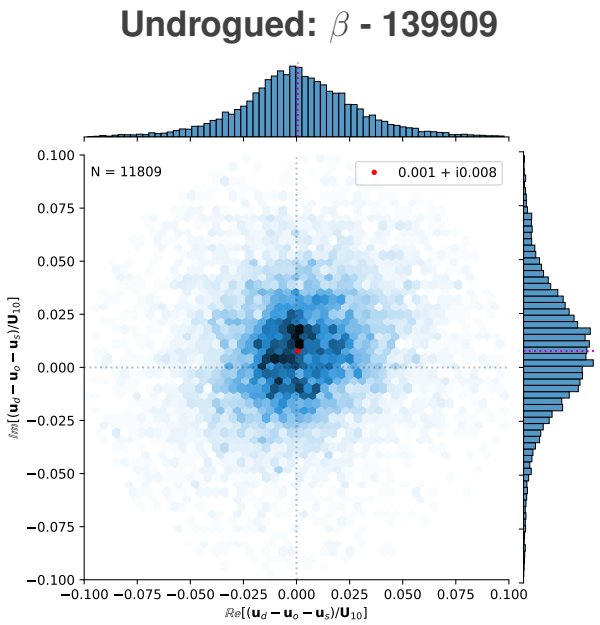

(b) 2D histograms of the leeway coefficients and the corresponding histograms for the along-wind and cross-wind components for drifter 139909 after drogue is lost. (a) $\boldsymbol{\alpha}$ forced with surface currents from ORAS5 and winds from ERA5. (b) $\boldsymbol{\beta}$ with the Stokes drift explicitly included from ERA5. Figures provided by Graig Sutherland.